

# Compliant Manipulator Design method

Applied for designing a 4-DoF manipulator with a TTTR-motion

**A.E. Huisjes**

Date:	28-1-2020
Supervisor:	Dr.ir. V. van der Wijk
Specialization:	MSD
Report no:	2020.006



# Compliant Manipulator Design method

## Applied for designing a 4-DoF manipulator with a TTTR-motion

MASTER OF SCIENCE THESIS

For the degree of Master of Science in Mechanical Engineering at Delft  
University of Technology

A.E. Huisjes

January 26, 2020

With supervision of Dr.ir. V. van der Wijk  
Chairman of the jury Prof. Dr.ir. J.L. Herder  
External jury member Dr.ir A.L. Schwab

Student no: 4173724  
Report no: 2020.006

Sept 2018 - January 2020

Precision and Microsystem Engineering - Mechatronic System Design  
Faculty of Mechanical, Maritime and Materials Engineering (3mE) · Delft University of Technology



---

# Table of Contents

<b>Acknowledgements</b>	<b>iii</b>
<b>1 Introduction</b>	<b>1</b>
1-1 The application field of mechanisms . . . . .	1
1-2 Mechanism demands from industry . . . . .	1
1-3 The advantages of compliant mechanisms over rigid-body mechanisms and their limitations	2
1-4 Goal of thesis: Methodological design approach for large range multi-DoF compliant mechanisms . . . . .	2
1-5 Thesis overview . . . . .	3
<b>2 The Compliant Manipulator Design (COMAD)-method</b>	<b>5</b>
2-1 Abstract and Introduction . . . . .	6
2-2 Theory of the COMAD-method . . . . .	7
2-3 Designing a TTTR-manipulator . . . . .	9
2-4 Concept selection . . . . .	11
2-5 Experimental evaluation . . . . .	14
2-6 Discussion and Recommendation . . . . .	17
2-7 Conclusion . . . . .	19
2-8 References . . . . .	19
<b>3 Discussion and conclusion</b>	<b>21</b>
3-1 Potential of unexplored designs . . . . .	21
3-2 Applications to gripper designs . . . . .	23
3-3 General multi-DoF compliant mechanism applications . . . . .	23
3-4 Conclusion . . . . .	23
<b>A Range of motion of a parallel mechanism with one, two and three legs</b>	<b>25</b>
<b>B Effect of geometrical conditions</b>	<b>29</b>
B-1 Geometrical condition-1 . . . . .	29
B-1-1 Geometrical condition-1: compliant mechanism stiffening. . . . .	31
B-2 Geometrical condition-2 . . . . .	32

---

<b>C</b>	<b>Curk models of conceptual CLS I-V</b>	<b>33</b>
C-1	Rotational deformation types . . . . .	35
C-2	manipulator cat. I . . . . .	36
C-3	manipulator cat. II . . . . .	37
C-4	manipulator cat. III . . . . .	38
<b>D</b>	<b>Conceptual variations in the configuration of the TTTR-manipulator</b>	<b>39</b>
<b>E</b>	<b>Manufacturing of COMAD-demonstrator</b>	<b>41</b>
E-1	Production method . . . . .	41
E-2	Selection of wires from the constraint topologies . . . . .	41
E-3	Design of the connection of the wires to the bodies . . . . .	44
E-4	Dimensioning . . . . .	45
E-5	Resulting demonstrator . . . . .	46
E-6	Experimental evaluation and test set up . . . . .	48
	<b>Bibliography</b>	<b>49</b>

---

# Acknowledgements

I would like to thank my supervisor dr. ir. Volkert van der Wijk for our discussion about dynamically balanced systems by which he convinced me about his mechanism design vision causing me to chose to start my thesis project about mechanism design. During our bright full, critical and open technical discussions he challenged me to deeply think about the current state-of-the-art material and try to solve the limitations. Bundling our knowledge has resulted in a project of what I am proud of. During our research, I get so excited about exploring new solutions that have not been shown before that it convinced me to proceed for another four years within the academic world as a Ph.D. researcher about compliant grippers. I would like to thank all the people (Tessa, Bram, Cas, Lola, Bas, Johan and Mart) who have reviewed parts of my written material which have improved my writing skills during this project. I would like to thank Bradly But who assisted me with the 3D prototyping of the demonstrator. I would like to thank my girlfriend for listening to all my brainstorm sessions about the project but especially for supporting me during difficult moments. Lastly, I would like to thank my parents for always supporting me during the decisions I have made during my studies.

Delft, University of Technology  
January 26, 2020

A.E. Huisjes



“We cannot solve our problems with the same thinking we used when we created them.”

— *Albert Einstein*



---

# Chapter 1

---

## Introduction

The purpose of this thesis is the presentation of the novel Compliant Manipulator Design (COMAD)-method for designing spatial multi-DoF compliant manipulators. The method has the aim to be an enhanced design method which includes parallel kinematic solutions by the "Type synthesis of legs"-technique and the FACT-method to obtain the complete compliant solution space. This chapter establishes the context of the research by presenting an overview of the application field, the state of the art, and the motivation of the goal of this thesis.

### 1-1 The application field of mechanisms

Every person uses multiple mechanical mechanisms on a daily basis, consciously or unconsciously. A mechanism is a mechanical device with the function to transfer a certain motion input into the desired motion output. For example, the mechanism within a door transfers the rotational motion of the human hand, which acts on the door handle, into a translational motion by which the door lock is moving inwards. The input of this mechanism is one rotational (R) Degree of Freedom (DoF) which is transferred into a translational (T) DoF of the output.

Humans are also supported by more complex mechanisms that have a multi-DoF input resulting in spatial motion pattern output at its end-effectors. These mechanisms are often included within robotic devices to provide the function of motion. A serial robotic arm (e.g. SCARA-robots), for example, is able to move the welding device (at its end-effector) in a six-dimensional space (3T and 3R) during repetitive welding processes of curved sheet plates within the car industry. Another application field of multi-DoF mechanisms is the packaging- or food-industry, for the automation of repeating pick and place processes (e.g. Delta-robots). These two examples intend to manipulate the spatial position of an object at its end-effector and they are therefore also known as manipulators. Manipulators are generally fixed to the ground to perform their intended tasks. This distinguishes them from the other field of robotic mechanisms, those which can freely move on the floor such as humanoid robots (e.g. the Atlas Robot from Boston Dynamics). Manipulator mechanisms are also used in the high-tech (e.g. semi-conductor) industry or during medical operations as they are able to provide very high precision placements and motions far beyond the limits of the human hand.

### 1-2 Mechanism demands from industry

Mechanisms are necessary within different applications, each requiring particular specifications. The food processing, high-tech and pick- and place-industry demand low cycle times because of a large throughput of objects per hour. The semiconductor industry requires very high precision of placement

and motion for the treatment of their products to result in a higher quality. Moreover, the high-tech, food, and medical industry operate in ultra-clean and or sterile environments thus demand mechanism solutions that do not pollute during their operation time and can be cleaned easily. At last, the food industry requires grippers that can handle soft, delicate, deformable and uniquely shaped objects such as fruits, vegetables, and meat.

### **1-3 The advantages of compliant mechanisms over rigid-body mechanisms and their limitations**

A rigid body (rb) mechanism is a linkage composed of rigid links and rb-joints. State-of-the-art rb-mechanisms cannot address the current demands of the industry such as high precision of motion and placement, being suitable to operate in clean environments, and low cycling times as they have three main limitations. Firstly of all, it is difficult for a rb-mechanism to achieve high precision as their motion relies on the sliding of contact surfaces at the rb-joints which requires a certain clearance [1]. Sliding causes friction, backlash, wear and high hysteresis thereby limiting the precision of these manipulators. Secondly, rb-mechanisms are not well suited for hygienic and ultra-clean environments as they are influenced by the wear and required lubrication [2]. Finally, rigid links of gripper mechanisms can cause harmful pressure spots at the surface of delicate, deformable objects because of the large grasping force that must withstand fast accelerations during the pick and place process of the food industry [2].

Compliant mechanisms are known to be advantageous for these applications because four reasons. First of all, they do not suffer from the undesirable effects of rb-mechanisms as their motion relies on the deformation of slender segments while being stiff in the constraint directions which results in excellent repeatable motion [3, 4, 5, 6]. Secondly, compliant mechanisms do not pollute during operating because they are friction-free which reduces wear and maintenance[2]. Thirdly, they are usually lighter and comprise fewer parts than rb-mechanisms or even result in a monolithic structure which makes them also easy to clean [2, 3]. At last, compliant mechanisms are deformable in their compliant direction which makes them capable to deform alongside the delicate objects while grasping [2]. Therefore, compliant mechanisms do offer high precision, light, and compact design and are suitable for (ultra)-clean environments.

However, one of the biggest limitations of compliant mechanisms is their relatively small range of motion (ROM), the reason why they still rarely implemented in multi-DoF mechanisms in the industry. The ROM of compliant mechanisms is limited by internal material stress and reducing constraint stiffness during deformation. Exceeding the material stress will cause plastic deformations of the material. The reduced constraint stiffness result in less load-carrying capacity and worse guided motions.

### **1-4 Goal of thesis: Methodological design approach for large range multi-DoF compliant mechanisms**

The goal of this thesis is to present a novel methodological design approach for multi-DoF compliant mechanisms with larger ROM and better stiffness capabilities. The Freedom and Constraint-Topology (FACT)-method and the Pseudo Rigid Body Model (PRBM)-method are two currently used state of the art methods for designing compliant mechanisms, however, the obtained designs from each method have limitations. By using the FACT-method, multi-axes flexure system solutions are obtained, however, spatial motion patterns consisting of translations in three dimensional directions can solely be realized using a set of serial stacked compliant topologies. Therefore, the kinematic solution space of the FACT-method remains limited to serial mechanisms instead of parallel legged compositions that conventional kinematic rb-design techniques can generate. By using the PRBM-method, designs are

obtained from an rb-mechanism that is synthesized in prior, either serial or parallel, using conventional kinematic rb-design techniques whereafter a compliant mechanism is obtained by replacing each rb-joint by an equivalent compliant hinge [3, 7, 8]. The resulting design are often not compact but heavy and bulky as they comprise of rigid links and compliant joints.

This thesis presents a new method, the Compliant Manipulator Design (COMAD)-method for designing multi-DoF compliant manipulators by considering them as an integrated multi-DoF compliant joint with either a serial or a parallel structure. First, the "type synthesis of Legs" techniques by Gosselin et al. [9] is used to obtain parallel legged kinematic solutions for the desired motion pattern. Different kinematic arrangements are possible for a given motion pattern because multiple DoFs of the legs are kinematically coupled to the motion directions of the end-effector. Despite that the complete parallel kinematic solution can not be obtained using the FACT method, it is possible to synthesize a multi-DoF flexure system for the leg of the mechanisms as it is one open serial kinematic chain composed with a set of DoFs. Subsequently, the FACT-method of Hopkins et. al. [10, 11] is used to obtain the multi-DoF flexure solutions for the legs which will be connected in parallel to result in the complete compliant solution space for the desired motion pattern.

## 1-5 Thesis overview

The ROM capabilities are challenging and will be discussed at the end of Chapter 2 because while designing such a multi-DoF manipulator not only do compliant mechanisms have a smaller ROM compared to a rb-mechanism, also the ROM of a rb-parallel mechanism is usually smaller than that of a rb-serial mechanism. On the other hand, a parallel mechanism generally have a higher stiffness in comparison with serial mechanisms which could improve the stiffness characteristics of the compliant mechanism hence could permits a larger ROM. Moreover, the resulting motion pattern of a parallel mechanism is obtained by the internal coupled motions within its parallel legs and, in order to result in a compact design, the full compliant potentials of the compliant mechanism must be used within multiple motion direction.

First, the theory is presented in Chapter 2.2, subsequently, it's applied for the design of a multi-DoF manipulator with TTTR-motion in Chapter 2.3 whereafter the best concept is selected and manufactured which is experimentally evaluated in Chapter 2.4 and 2.5. The results and findings are discussed in Chapter 2.6 whereafter the conclusion is presented in Chapter 2.7. Finally, in Chapter 3, the performance and potentials of the COMAD-method are discussed concerning the demands of the industry and recommendations for further research are provided.



---

Chapter 2

---

# **The Compliant Manipulator Design (COMAD)-method**

# The Compliant Manipulator Design (COMAD)-method - applied for the design of a spatial 4-DoF TTTR compliant manipulator with a large range of motion.

---

## Abstract

Current multi-DoF compliant manipulators are still rarely implemented in the industry because their range of motion (ROM) is limited as their designs are heavy and bulky or obtained by a serial set of multiple stacked flexure systems, which limits their compactness. The goal of this article is to overcome these limitations by considering them as an integrated multi-DoF compliant joint, either serial or parallel, and setting up a new method the Compliant Manipulator Design (COMAD)-method and investigate its performance. This method will combine the "Type synthesis of legs"-technique to include parallel kinematic solutions for the desired motion pattern whereafter the complete compliant solution space is obtained using the FACT-method. The method is applied for designing a 4-DoF-manipulator with a TTTR-motion pattern resulting in four new concepts composed of compactly aggregated wire flexures. After the concept selection, a demonstrator is manufactured which excellently possesses four decoupled motions with a relatively large ROM. This can be seen as a new milestone for designing multi-DoF compliant manipulators as it permits a larger ROM and better stiffness capabilities than those obtained from conventional methods because all compliant topologies are deflecting in series due to the parallel kinematic couplings within the multi-DoF flexure systems.

---

## 1. Introduction

Nowadays, more than 2 million robots are used in the industry for the automation of repeating processes [1]. For example, pick and place robots that pick up an object (e.g. a chip), move it to another location, change its orientation, and release it for the next step of the production process [2]. These spatial robotic devices that grasp and move a particular object are generally called manipulators. These manipulators possess a relatively large motion pattern comprising three Translations and one Rotation (TTTR-motion pattern) [3]. The high-tech industry in particular demands low cycle times and a high precision of placement. However, the motion of current manipulators relies on the sliding of contact surfaces at the rigid body (rb)-joints which requires clearance [4]. Sliding causes friction, backlash, wear and high hysteresis thereby limiting the precision of these manipulators.

Compliant mechanisms are known to be advantageous because they do not suffer from these undesirable mechanical effects. Unlike conventional joints, the motion of compliant joints relies on the elastic deformation of slender segments resulting in an excellent repeatable motion while also minimizing the mass and costs [5–8]. Moreover, compliant mechanisms do not need lubrication which is necessary for operating in the ultra-clean environments of the high-tech- and food industry. However, they are still rarely implemented as a pick and place manipulator due to their small range of motion limited by internal material stress and reducing constraint stiffness during deformation. This restricts the range of motion of compliant mechanisms compared to rb-mechanisms.

Mainly two methods are used for designing compliant mechanisms. The first method is the Pseudo Rigid Body Model (PRBM)-method [5, 9, 10] where a compliant mechanism is obtained based on an rb-mechanism that is synthesized using conventional kinematic rb-design techniques. The rb-mechanism contains rigid links connected by rb-revolute or rb-prismatic joints. An equivalent compliant mechanism is obtained by replacing these rb-joints by comparable compliant joints [5]. The resulting compliant mechanism, either serial or parallel, aims to mimic the kinematic behavior of the original rb-mechanism.

The second method used for designing compliant mechanisms is the Freedom and Constraint Topology (FACT)-method [11]. The FACT-method aims at the synthesis of multi-DoF flexure systems for a required motion pattern. The general layout of the flexure system is based on the constraint topology which contains the position and orientation of the constraints that restrict the connected body for a desired motion pattern. Hopkins et. al. have defined the "parallel pyramid" (from now on referred to as "pyramid") which includes 26 different motion patterns that can be obtained by a flexure system composed of a single constraint topology containing parallel wire flexures.

It is not possible to obtain a motion pattern comprising translations into three dimensional directions by one single topology composed out of parallel wire flexures hence, they are not included by the "pyramid" [11, 12]. This is since the connection of the first wire flexure (modeled with one infinite stiff axial direction) between the body and the ground will already constrain one of its three translational DoF. A solution for motion patterns that are excluded

from the "pyramid", is to create a serial set of multiple stacked flexure systems [13]. However, literature already presents rb-parallel legged mechanisms which are having a larger variety of kinematic solutions for a desired motion pattern compared to serial mechanisms. Therefore, the kinematic solution space of the FACT-method is limited because no solutions can be obtained based on parallel kinematic solutions.

The PRBM-method is not suitable to obtain compact multi-DoF designs due to the individual replacement of each joint. The resulting compliant mechanism is a linkage of rigid links and compliant joints which makes them heavy and bulky, while the kinematics obtained by this architecture might be integrated further into a compact multi-DoF flexure system.

Therefore, it is proposed in this article to consider the manipulator not as a mechanical linkage but as an integrated multi-DoF compliant joint, either serial or parallel.

The goal of this article is to set up a new method for designing spatial multi-DoF compliant manipulators with a relatively large ROM using the "Type synthesis of Legs" and the FACT-method and investigate its performance: This method will be referred to as the Compliant Manipulator Design (COMAD)-method.

The "Type synthesis of Legs" - techniques by Gosselin et al. [3] are used to synthesize the complete kinematic solution space for the required motion pattern. The obtained legs can be seen as open serial kinematic chains with a set of DoF for which a compliant flexure system can be obtained using the FACT-method of Hopkins et. al. [11, 13]. This results in the complete compliant solutions space for the manipulator (to the best of the authors knowledge).

With this approach, the architecture of the manipulator will comprise compactly aggregated flexible elements with parallel coupled kinematic relations. Due to these coupled relations, the flexible elements will have a common contribution to each primary motion- and constraint-direction of the end-effector resulting in a large ROM and a better stiffness capabilities.

First, the theory of the COMAD-method will be presented in section 2. Subsequently, the method is applied for designing a 4-DoF spatial compliant manipulator with a  $T_x T_y T_z R_z$ -motion pattern. For this purpose, the kinematic solution space is synthesized in section 3 whereafter multi-DoF flexure systems are obtained resulting in the compliant solution space. The best concept is selected in section 4 and subsequently manufactured as a demonstrator which is experimentally evaluated in section 5. The results are discussed in section 6 whereafter the conclusion is presented in section 7.

## 2. Theory of the COMAD-method

The COMAD method starts with the required motion pattern and consists of two consecutive steps that proceed downwards in Figure 1. The required motion pattern comprising a number of  $i$  translational DoF and  $j$  rotational DoF and presented as  $\mathcal{T} = i\mathbf{T} - j\mathbf{R}$ . The first step is obtaining the kinematic solution space for the required motion which results in a chained set-of-DoFs. As seen, result this step in a bifurcation to the left side, "serially chained" for serial mechanism solutions, and the right side, "parallel legged" for the legs of a parallel mechanism, of which an example of each mechanism is presented in Figure 2 and Figure 3 respectively. The second step is the obtain the compliant solutions for each chained set-of-DoF what could result in a flexure system of one, (a) and (c), or multiple serial topologies, (b) and (d).

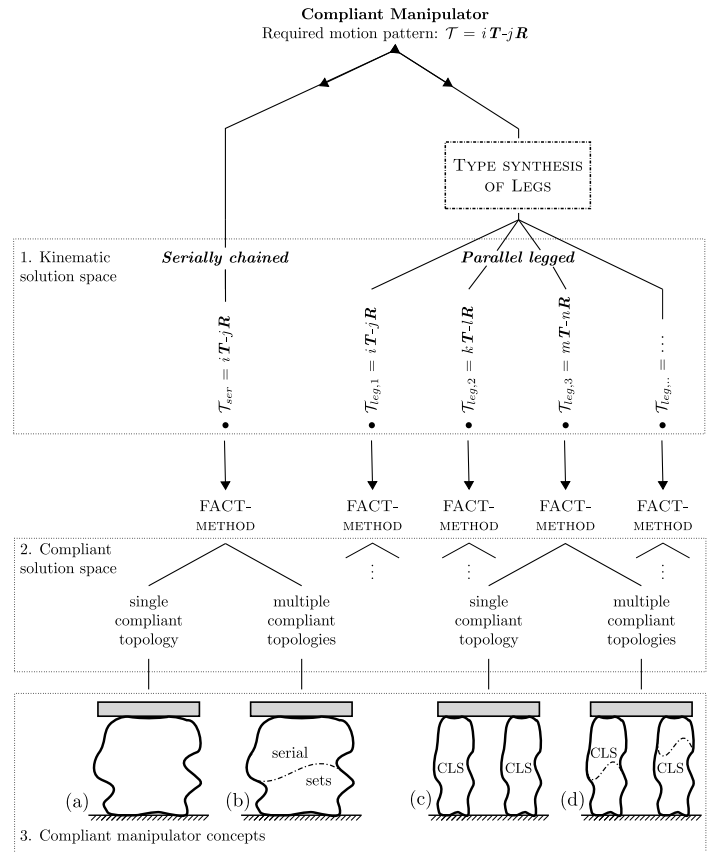


Figure 1: The Compliant Manipulator Design (COMAD)-method: First, the complete kinematic solution space is synthesized for the required motion pattern  $\mathcal{T} = i\mathbf{T} - j\mathbf{R}$  for the manipulator which contains both the serially chained and parallel legged solutions (here,  $i, k, m$  and  $j, l, n$  are the number of Translational and Rotational DoFs). Subsequently, a compliant solutions of a single compliant topology (a) and (c) are attempt to be obtained for each kinematic solution, otherwise it result in multiple compliant topologies (b) and (d). The compliant solutions that are having equal kinematics as  $\mathcal{T}_{leg}$  are called Compliant Leg Solutions (CLS). The compliant manipulator concepts are created by connecting multiple CLSs in parallel to the end-effector.

### 2.1. The kinematic solution space

The kinematic solution could comprise an open- or a closed chain which identifies the mechanism architecture and contains the number of prismatic and revolute joints, and their orientation w.r.t. each other. In Figure 2 and 3 an example of an rb-serial mechanism and an rb-parallel mechanism is presented, both possessing a  $\mathcal{T} = 3\mathbf{T} - 1\mathbf{R}$  motion pattern. The end-effector of a serial mechanism is connected to the ground by one open serial chain of rb-joints while the end-effector of parallel mechanisms is connected to the ground with multiple parallel chains, called legs.

This results in two different types of kinematic solutions, a serially chained kinematic solution or a parallel legged kinematic solution. A serial kinematic solution is equal to the sum of all DoF contained by the chain [13]. Each prismatic joint has one translational (T)-DoF and each revolute joint one rotational (R)-DoF. Hence, in general the serially chained kinematic solution is an open-chain composed of a set-of-DoF containing an equal number ( $i$  and  $j$ ) of T-DoFs and R-DoFs as the required motion pattern:  $\mathcal{T}_{ser} = i\mathbf{T} - j\mathbf{R}$  as presented in scheme of Figure 2.

For parallel mechanisms are the constraint directions of the end-effector equal to the sum of all constraint directions which are obtained by its legs [3]. Using "The type-synthesis of Legs" all possible "legtypes" are synthesized that are having one or all of the required constraints. These legtypes containing a set-of-DoF and are listed for each spatial motion pattern in [3] which are the parallel kinematic solutions  $\mathcal{T}_{leg}$  of the scheme of Figure 1. Multiple parallel kinematic solutions are presented because a particular set of constraints can be obtained by a variety of legtype arrangements each composed of a different num-

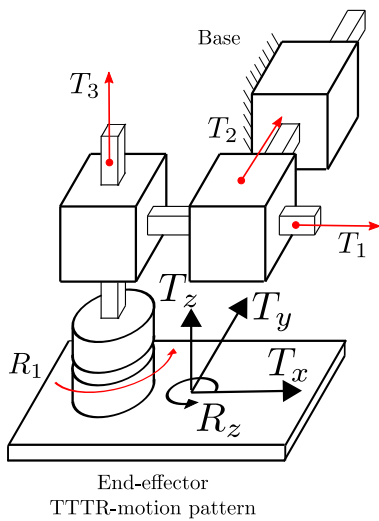


Figure 2: Rigid body serial mechanism with a TTTR-motion pattern. It contains three differently oriented prismatic joints plus one revolute joint in series. The serially chained kinematic solution is an open-chain composed of a set-of-DoF containing an equal number 3 T-DoFs and 1 R-DoFs.

ber of ( $i, k, m$ ) T- and ( $j, l, n$ ) R-DoF. The set-of-DoF of each legtype must satisfy certain geometrical conditions to orient the constraints in the desired directions and to have a movable mechanism.

For example, the two legs of the parallel mechanism of Figure 3 are encircled by the striped lines and containing a set of two differently oriented prismatic joints plus two revolute joints in series. The leg in this example is legtype  $\mathcal{T}_{leg} = 2\mathbf{T}2\mathbf{R}$ . The sum of the constraints obtained by its set of joints prevents a rotation around the x- and y-axis. Hence, two rotations of the end-effector are constraint while its free to move in the remaining three translational directions and one rotation. Each primary motion direction of the end-effector is kinematically coupled to a simultaneous motion of a set of internal DoFs of both legs. For example, the translational motion in the y-direction is obtained by a simultaneous rotation of all R-joints plus a translation of  $T_1$  and/or  $T_2$ .

### 2.2. The compliant solution space

The second step of the method is synthesizing the compliant solutions for the kinematic solution space, using the FACT-method. When the entire set-of-DoF of a kinematic solution is included by the "pyramid" it can be obtained by a single compliant topology, (a) and (c), otherwise a flexure system solution of  $n$  serial compliant topologies is required, (b) and (d). For this, the set-of-DoF must be distributed over chain that contains a serial set of  $n$  elements. A kinematic solution results in multiple compliant solutions when its set-of-DoF is included by the "pyramid" multiple times. Each compliant solution is a different arrangement of the required constraints.

The compliant solutions of a parallel kinematic solution, thus towards (c) and (d), must be validated if they

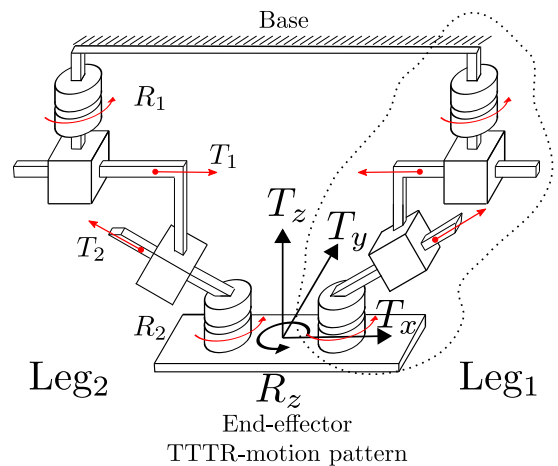


Figure 3: Rigid body parallel mechanism with a TTTR-motion pattern: two legs (comprising of 2 T-DoFs and 2 R-DoFs) connected in parallel to the end-effector. The TTTR-motion pattern is provided by a simultaneous motion of the legs DoF because of the parallel kinematic coupling between them. Using the "The type-synthesis of Legs" all possible parallel legged kinematic solutions  $\mathcal{T}_{leg}$  of the scheme of Figure 1 are obtained for a given motion pattern [3].

satisfy the geometrical conditions, in order to guarantee that they possess equal kinematics as the rb-legtype. Those who satisfy are called the Compliant Leg Solutions and proceed towards the next step of the scheme (c) and (d). The final step is to orient the CLS in-line with the required motion pattern and connect them in parallel to the end-effector which results in a compliant manipulator concept.

### 3. Designing a TTTR-manipulator

Serial Scara-robots and parallel Delta-robots are examples of frequently-used manipulators and their development goes back to the 1970s and 1980s [3]. Since then, mainly iterations of their sub-components have been done while the industry's demand for a higher precision increases rapidly. The mechanisms are relatively voluminous to permit a relatively large spatial motion pattern in order to fulfill its tasks. The cycle time is limited because they need a lot of kinetic energy for their own movements in comparison with the movements of the end-effector. In addition, the precision of these mechanisms is limited because they are composed of rb-joints which makes them also relatively heavy and spacious. Hence, a useful and challenging design case is to design a compact 4-DoF compliant manipulator with a relatively large spatial  $T_x T_y T_z R_z$ -motion pattern using the COMAD-method.

#### 3.1. The kinematic solution space

The serial solution is a set-of-DoF that contains similar DoF as the **TTTR**-motion pattern hence, an open-chain containing a set-of-DoF  $\mathcal{T}_{ser} = 3T - 1R$ . This result is presented in the first column of Table 1 and the kinematics are visualized in Figure 2.

The parallel legged kinematic solutions are synthesized using "the type synthesis of legs"-techniques and listed [3]. The resulting legtypes are composed of a set-of-4-DoF and a set-of-5-DoF. In the first instance, the 5-DoF legtypes are omitted because a set of lower DoF can be obtained by a lower number of constraint topologies and thus results in a more compact united compliant manipulator. The 4-DoF legtypes are listed below and presented in the second, third and fourth column of Table 1:

- Legtype 1,  $\mathcal{T}_{leg.1} = 3T1R$
- Legtype 2,  $\mathcal{T}_{leg.2} = 2T2R$
- Legtype 3,  $\mathcal{T}_{leg.3} = 1T3R$

The **TTTR**-motion pattern is only obtained when these legtypes are connected in parallel to the end-effector and as long as their set-of-DoF satisfy the two geometrical conditions (G). The geometrical conditions corresponding to these legtypes are listed [3] and stated below:

- G1) The axes of all R-DoF are always parallel.
- G2) The direction of at least one T-DoF is not perpendicular to the axes of the R-DoF.

Geometrical condition-1 (G1) must be satisfied to have a movable parallel mechanism. All "rigid links" are moving in the same plane because all R-axes are parallel as is shown in Appendix B.

Geometrical condition-2 (G2) must be satisfied to have translational motion in all spatial directions. This can be explained using Figure 3, because  $R_1$ ,  $R_2$  and  $T_1$  are related to the position of the end-effector in the xy-plane. In order to have a translation in spatial direction, must  $T_2$  be directed out of this plane, thus in the z-direction, as is shown in Appendix B.

#### 3.2. The compliant solution space

In the second step of the COMAD-method the compliant solutions are synthesized for the kinematic solution space. First, an attempt is to obtain a compliant solution of a single topology for each kinematic solution, (a) and (c). Therefore, the complete 4-DoF-set of each kinematic solution will be handled while using the FACT-method. This procedure is shown in Table 1.

The 4-DoF-set (**3T1R**) is not included by the "pyramid" and therefore not be obtained by one constraint topology such as shown in the first and second column of Table 1. The 4-DoF-set of (**2T2R**) and (**1T3R**) are contained by the "pyramid" and can be obtained by the three listed constraint-space-topologies which are listed in the third and fourth column of Table 1. The names of these constraint topologies are corresponding to a particular constraint space that can be found in the "pyramid". However, none of the topologies is satisfying the geometrical condition-1 because each of them has intersecting rotational axes. Hence, no compliant manipulator concepts of a single topology could possess the TTTR-motion pattern and, therefore, the manipulator must be composed of multiple serial compliant topologies.

The second attempt is to obtain compliant solutions comprising a minimum number of  $n = 2$  serial topologies

Table 1: The integration of the serially chained kinematic solution into a compliant concept: of a single topology (first column) as reported by subsection (a), or of a serial set of multiple  $n = 2$  topologies (2,3,4-th columns) as reported by subsection (b).

	$\mathcal{T} = 3T1R$			
	ser. kin.	legtype-1	legtype-2	legtype-3
Resulting kinematic solutions	<b>3T1R</b>	<b>3T1R</b>	<b>2T2R</b>	<b>1T3R</b>
Required FACT-topologies	<i>multiple</i>	<i>multiple</i>	<i>single</i>	<i>single</i>
Constraint space solution(s)	×	×	<b>4DOF-2</b>	<b>4DOF-(1,3)</b>
Leg meets geo. cond.	N.A.	×	×	×

Table 2: Integration of legtype 1, 2 and 3 (Table 2.1, 2.2 and 2.3) into compliant concepts composed of a serial set of  $n=2$  multiple topologies, as reported by subsection (d). Chain 3 of Table 2.1 results in Compliant Leg Solution 1 (CLS I). Chain 1 of Table 2.2 results in CLS II-V.

Required twist system	$\mathcal{T}_{leg,1} = 3T1R$			$\mathcal{T}_{leg,2} = 2T2R$				$\mathcal{T}_{leg,3} = 1T3R$		
	chain 1	chain 2	chain 3	chain 1	chain 2	chain 3	chain 4	chain 1	chain 2	chain 3
Resulting kinematical serial set(s)	<b><i>TT</i></b> <b><i>TR</i></b>	<b><i>TTT</i></b> <b><i>R</i></b>	<b><i>TTR</i></b> <b><i>T</i></b>	<b><i>TR</i></b> <b><i>TR</i></b>	<b><i>TT</i></b> <b><i>RR</i></b>	<b><i>TTR</i></b> <b><i>R</i></b>	<b><i>TRR</i></b> <b><i>T</i></b>	<b><i>TR</i></b> <b><i>RR</i></b>	<b><i>RRR</i></b> <b><i>T</i></b>	<b><i>TRR</i></b> <b><i>R</i></b>
Required FACT-topologies	<i>multiple</i> <i>single</i>	<i>multiple</i> <i>single</i>	<i>single</i> <i>single</i>	<i>single</i>	<i>multiple</i> <i>single</i>	<i>single</i> <i>single</i>	<i>single</i> <i>single</i>	<i>single</i> <i>single</i>	<i>single</i> <i>single</i>	<i>single</i> <i>single</i>
Constraint space solution(s)	×	×	<b>3DOF-2</b> <b>1DOF-3</b>	<b>2DOF-</b> <b>(2,8,9)</b>	×	<b>3DOF-2</b> <b>1DOF-1</b>	<b>3DOF-1</b> <b>1DOF-3</b>	<b>2DOF-(..)</b> <b>2DOF-1</b>	<b>3DOF-(3,8)</b> <b>1DOF-3</b>	<b>3DOF-(..)</b> <b>1DOF-3</b>
Leg meets geo. cond.	×	×	✓	✓*	×	×	×	×	×	×

Table 2.1

Table 2.2

Table 2.3

to have the compliant manipulator as compact as possible and to reduce the required number of intermediate bodies that are necessary for connecting the serial topologies. The entire set-of-4-DoF can be divided over a chain with two serial-subset comprising two elements which can be a 3-DoF- plus a 1-DoF- element or a 2-DoF- plus a 2-DoF-element. The resulting chain of the serially chain kinematic solutions are listed in Table 3. Both elements of chain-3 (***TTR***)(***T***) are contained by the "pyramid" and thus obtained by single constraint topologies. Element (***TTR***) is obtained by topology-**3DOF-2** and element (***T***) by topology-(**1DOF-3**). The geometrical layout of both compliant topologies are presented in the first and second column of Figure 4, and the resulting serial compliant manipulator concepts-I in the third column.

The distribution of the 4-DoF-set associated with legtype-1, legtype-2, and legtype-3 over the chain with two serial-subset are listed in Table 2.1, 2.2 and 2.3. Most of them are rejected by three reasons.

Table 3: The integration of the synthesized 4-DoF-legtypes of the parallel kinematic solutions into a compliant concept of a single topology, as reported by subsection (c).

Required kin. sol.	$\mathcal{T}_{ser} = 3T1R$		
	chain-1	chain-2	chain-3
Resulting serial set	<b><i>TT</i></b> <b><i>TR</i></b>	<b><i>TTT</i></b> <b><i>R</i></b>	<b><i>TTR</i></b> <b><i>T</i></b>
Required FACT-topologies	<i>multiple</i> <i>single</i>	<i>multiple</i> <i>single</i>	<i>single</i> <i>single</i>
Constraint space solution(s)	×	×	<b>3DOF-2</b> <b>1DOF-3</b>

First, each chain having an element (***TT***) or (***TTT***) is rejected because these elements are not included by the "pyramid" thus require multiple FACT-topologies.

Second, each chain having an element (***RR***), (***RRR***) or (***TRR***), are rejected because they do not satisfy the geometrical condition-1. These elements having 2 R-DoF but their constraint space has two intersecting R-axes.

At last, three chains are rejected because they do not satisfy geometrical condition-2 among the serial elements while satisfying geometrical condition-1. Chain-3 of legtype-2, because **3DOF-2** has 2-T-DoF which are perpendicular to its own R-DoF-axis as well to the R-axis of **1DOF-1**. Chain-1 of legtype-2 can be obtained by 6 different combinations of serial-topologies, because the (***TR***) element can be obtained by compliant topologies **2DOF2**, **2DOF8** and **2DOF9**. Each compliant solution is a combination of the three constraint spaces. However, compliant solution (**2DOF2**)(**2DOF**) and (**2DOF8**)(**2DOF8**) are rejected because they do not satisfy geometrical condition-2 among both serial elements while their R-axes are oriented parallel.

The remaining four compliant solutions of legtype-2 and chain-3 of legtype-1 do satisfy both geometrical conditions. Hence, these five solutions are proceeding downwards in Figure 1 to (d) because they are CLSs which are having equal kinematics as the synthesized parallel legtypes.

To conclude, the five CLSs are listed below and a representation of the geometrical layout is given in the third column of Figure 4. Compliant manipulators that possess the ***TTTR***-motion pattern are generated by connecting multiple CLSs in parallel to the end-effector.

- I. (**3DOF-2**)(**1DOF-3**)
- II. (**2DOF-9**)(**2DOF-9**)
- III. (**2DOF-9**)(**2DOF-8**)
- IV. (**2DOF-9**)(**2DOF-2**)
- V. (**2DOF-8**)(**2DOF-2**)

## 4. Concept selection

This section will look at how the TTTR-manipulator concepts are obtained by specifying the position, oriented and the parallel connection of the five CLSs-concepts. Subsequently, the concept with the largest ROM will be selected.

### 4.1. Design of Compliant Leg Solutions configuration

All synthesized CLS of Figure 3 are able to perform the 3T1R-motion pattern, however, the orientation and placement of their topologies is still undefined and, therefore, the directions of the motion pattern as well. It requires two steps to define the spatial placement of the topologies such that they possess the motion pattern in the required direction  $T_x T_y T_z R_z$ .

The first step is that each topology provides a set of six free design variables determine their placement in space, w.r.t. ground and end-effector. Each topology is presented in the left and middle column of Figure 4 for their initial orientation angle (for the value  $0^\circ$ ) and in the lower row two boxes are added below each column representing the topologies with their design variables. The spatial location of each topology w.r.t. the ground is determined by  $\mathbf{r} = (r_x, r_y, r_z)$  and the orientation angle w.r.t. the ground by yaw  $\psi$ , pitch  $\theta$  and roll  $\phi$ . Topology **2DOF-9** has a seventh design variable, the internal angle  $\beta$  between the ground and the plane (with intersecting constraint lines) [11] and is shown in Figure 4. The serial sequence of topologies in the CLS is free to choose, but the design variables of the topology connected to the ground are labeled with  $(\ )_1$ , and those of the topology connected to the end-effector with  $(\ )_2$ .

The second step is that three design actions are defined based on the geometrical conditions of the legtypes and the required directions of the motion pattern which are listed below. These design actions are required to guarantee that the manipulator concepts will possess the  $T_x T_y T_z R_z$ -motion pattern. Design action A1 results that the end-effector has rotational DoF around the  $R_z$ -axis while geometrical condition-1 is covered simultaneously. Design action A2 results that the number of T-DoF contained by 4-DoF-set of the CLS are performed in all required dimensions because it avoids a redundant DoF. Design action A3 is similar as geometrical condition-2 but now reformulated w.r.t. the ground. The three specific design actions, A, for each topology are defined as follows:

- A1) The rotational axis of each topology must be oriented parallel to the Z-axis.
- A2) The translational DoF of both topologies within the same CLS may not be oriented in the same direction.
- A3) At least one T-axis is not perpendicular to the Z-axis.

Certain design variables will be specified into fixed design parameters using these design actions. For example,

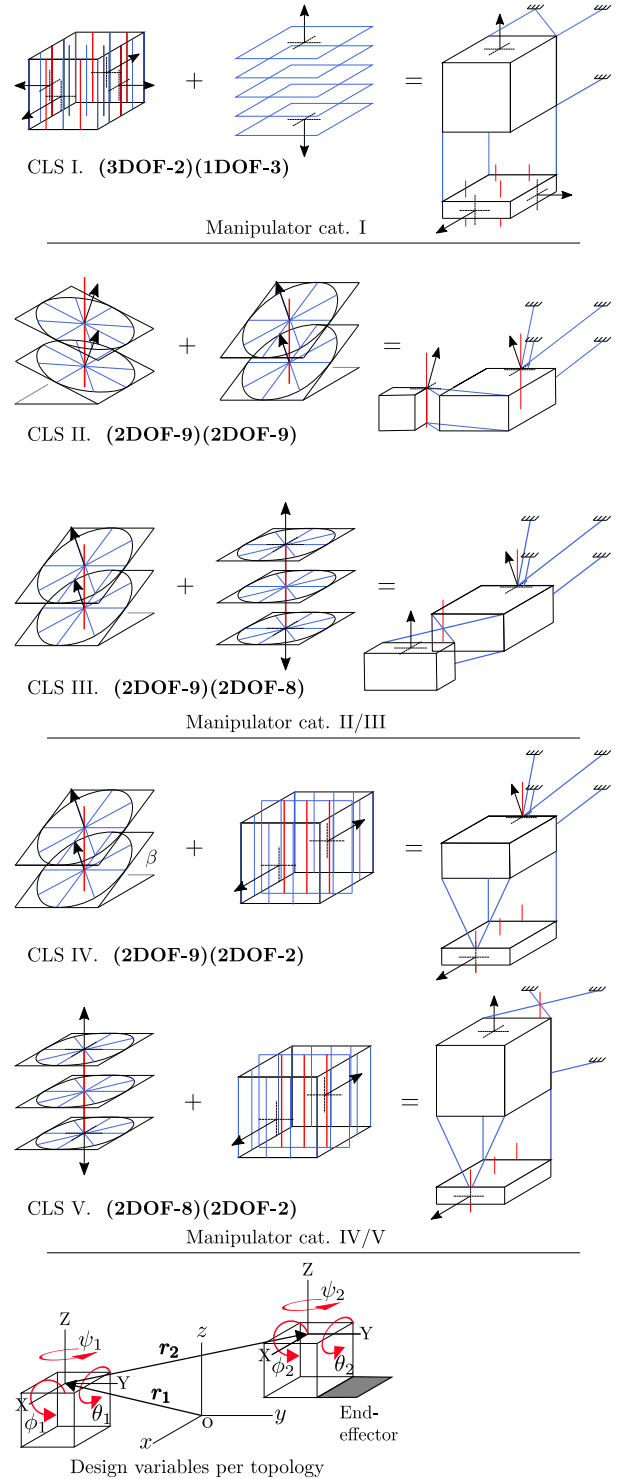


Figure 4: Compliant Leg Solutions (CLSs) I-V, right column. Each CLS is composed of  $n=2$  serial topologies, left and middle column. Blue line is constraint line, red line is R-DoF axis, black arrow is T-DoF. Bottom row, six design variables per topology to determine their location  $\mathbf{r} = (r_x, r_y, r_z)$  and orientation angle  $\psi, \theta, \phi$  w.r.t. the ground. The topologies are orientated in their initial design value for their orientation  $\psi = \theta = \phi = 0^\circ$ . The five CLSs are clustered in categories cat. I, cat. II/III, cat. IV/V based on similarities in kinematics and deformation

design action A1 fixates the pitch and roll as  $\theta = \phi = 0^\circ$  for those topologies which contain an R-DoF to orientated their R-axis in the Rz-direction. The specified design parameter of each topology is listed below per CLS concept:

Design action A1 fixate:

- for CLSs I-V the pitch and roll to  $\theta = \phi = 0^\circ$  for the topologies **3DOF-2**, **2DOF-9**, **2DOF-8** and **2DOF-2**.

Design action A2 fixate:

- for CLS-I the  $\phi = \theta \neq 90^\circ \neq 270^\circ$  for topology **1DOF-3**.
- for CLS-II the internal angle  $\beta_1 \neq \beta_2$  if  $\psi_1 = \psi_2$  or  $\psi_1 \neq \psi_2$  if  $\beta_1 = \beta_2$  for both **2DOF-9**-topologies.
- for CLS-III the  $\beta \neq 0^\circ \neq 180^\circ$  for topology **2DOF-9**.
- for CLS-IV the  $\beta \neq 90^\circ \neq 270^\circ$  for topology **2DOF-9**.

After these design variables have been specified, design action A3 only fixate:

- CLS-II, the  $\beta_1 \neq 0^\circ$  or  $\beta_2 \neq 0^\circ$  for both **2DOF-9** topologies.

The remaining free design variables can be varied to change the configurations of the manipulator concepts while satisfying the  $\mathbf{T}_x\mathbf{T}_y\mathbf{T}_z\mathbf{R}_z$ -motion pattern.

#### 4.2. Design of the manipulator configuration

While orientating and attaching the legs to the end-effector, the aim is to achieve a symmetrical design because this is advantageous for its mechanical behavior. Certain mechanical properties, either static or dynamical, compensating each other at both sides of the symmetry line because the kinetics and kinematics are equal but opposite. For example, a symmetric design has an equal distribution of mass [14], a compensation of the bending moment and the cancellation of vibrations among the symmetry line. In addition, the kinematics of the DoF at both sides of the symmetry line coupled to each other. A variation in a DoF on one side results in an opposite but equal variation of the mirrored DoF on the other side. Therefore, less actuation is required to control each DoF of such a symmetric design.

Each leg can be connected at a different side of the end-effector or all at the same side because none of the design variables which specify the location  $\mathbf{r} = (r_x, r_y, r_z)$

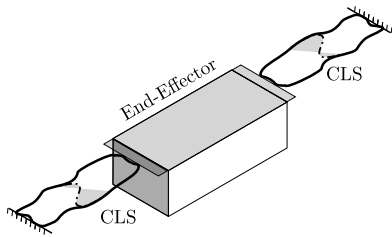


Figure 5: Manipulator concept configuration (symmetric): Two legs (CLS) with mirrored orientation, parallel connected at opposite sides of the end-effector.

are fixed. Also, the orientation of each topology around the z-axis,  $\phi$ , is a free design variable, hence two legs can have the same orientation or be mirrored w.r.t. each other such as shown in Figure 6 and Figure 5, respectively. The design with the mirrored leg orientation is symmetric and, therefore, be selected as manipulator concept.

It is decided to use two legs for the ease of manufacturing and because more legs will probably limit the ROM. As is shown in Appendix A, results the addition of a third leg to the end-effect a limitation in the ROM normal to that leg because the links of the third leg become fully stretched. Without the third leg, the ROM in this direction is larger.

Given these points, the manipulator concepts will be constructed out of two CLSs which are attached at the two opposite sides of the end-effector, in a mirrored orientation  $\phi = 180^\circ$  w.r.t. each other resulting in a symmetrical design.

#### 4.3. Concept selection

The legs are connected in parallel resulting in five compliant manipulator concepts which are divided into three categories based on similarities in their kinematic- and deformational behavior. First, a category will be selected and subsequently a specific concept of that category. An enumeration and a brief explanation of the three categories is stated below. The extended kinematic analysis can be found in Appendix C.

**manipulator cat. I:** *One topology of the leg is deforming in the DoF similar as the displacement direction of the end-effector.*

**manipulator cat. II/III:** *Both topologies of the leg are bending in their R-DoF during a displacement in the Ty-direction of the end-effector.*

**manipulator cat. IV/V:** *One topology deforms due to torsion and one due to bending both in their R-DoF during a displacement in the Ty-direction of the end-effector.*

##### 4.3.1. Concept category selection

The manipulator cat. I is rejected because it has a smaller ROM compared to manipulator cat. II/III or ma-

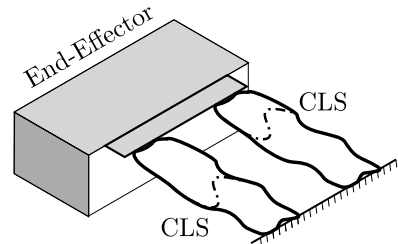


Figure 6: Manipulator concept configuration: Two legs (CLS) with the same orientation, parallel connected at the same side of the end-effector.

nipulator cat. IV/V. The total displacement in the primary motion directions of the end-effector is equal to the sum of the deflections of both serial topologies in each leg [13]. Only one topology is deforming in manipulator cat. I and therefore only one deflection is contributing to the displacement of the end-effector, while for comparison, the other categories have a summed contribution of both serial deflecting topologies.

The kinematics of manipulator cat. II/III and category manipulator cat. IV/V are obtained by the same parallel kinematic solution  $\mathcal{T}_{leg,2} = 2\mathbf{T}2\mathbf{R}$  as the rb-mechanism in Figure 3. First, the configuration of the concepts is selected which permits the largest ROM with the purpose of equal comparison of the categories whereafter the best one is selected. Although the kinematic solutions are the same as the rb-mechanism in Figure 3 certain effects corresponding to the deformation by bending and torsion will influence the mechanical behavior of the mechanism.

#### 4.3.2. Concept selection within cat. II/III

Two manipulator concepts of manipulator cat. II/III are presented in Figure 8 and 9.

The first concept is the straight-legged-concept, it has both topologies aligned (the design variables are orientated as  $\phi_1 = \phi_2 = 0^\circ$ ) and is shown in Figure 8. Stiffening of the manipulator occurs during a motion in the  $T_y$ -direction because the left leg is pulling the end-effector to the left while the right leg is pulling the end effector to the right. The body which is connected to topology **2DOF-8** or **2DOF-9** orbits in a circular path around the rotational axis. The circular red path caused by bending is presented in the left side of Figure 7. It results in a clockwise rotation of the box while simultaneously greatly translating the box in the  $y$ -direction, away from the  $R$ -axis, and slightly translating it in the  $x$ -direction, towards the  $R$ -axis in the direction of the bigger black arrow. These translational components in the  $x$ -direction are also depicted as a black arrows in Figure 8. As a consequence, the left leg is pulling the end-effector to the left while the right leg is pulling the end effector to the right.

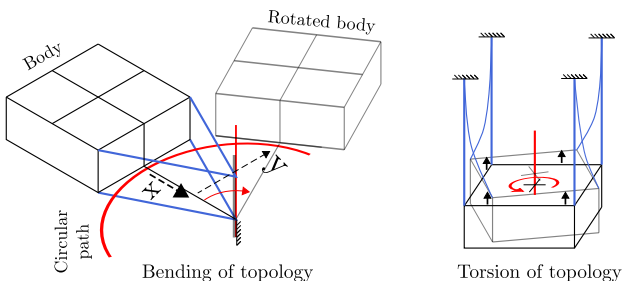


Figure 7: The rotational twist occur by bending of the compliant topology (left) or by torsion of the compliant topology (right). Bending: the body orbits in a circular path in the XY-plane and has a translational  $T_y$ - and  $T_x$ -component (towards the  $R$ -axis). The direction of the  $R$ -axis is compliant and the radial direction stiff. Torsion: the body pivots on its own axis, is compliant in radial direction and stiff in axial direction.

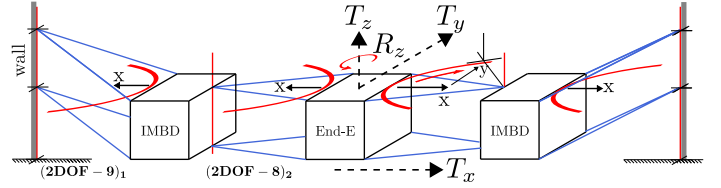


Figure 8: Manipulator concepts cat. II/III: Straight version with aligned topologies.

The second concept is the flipped-legged-concept whereby both topologies are flipped and stacked above each other (the design variables are orientated as  $(\phi_1 = 0, \phi_2 = 180^\circ)$ ) and is shown in Figure 9. This configuration of the topologies allows for a large ROM in the  $T_y$ -direction because both topologies of the leg are bending in an inverse direction. Hence, the translational components in the  $x$ -direction of the circular paths are equal but opposite and therefore cancel each other out.

Therefore, the flipped-legged-configuration is the selected concept of manipulator cat. II/III for comparison with manipulator cat. IV/V.

#### 4.3.3. Concept selection within cat. IV/V

Two manipulator configurations of cat. IV/V are the hanging and the standing version which are presented in Figure 11 and 10, respectively. The hanging version is selected because it has a higher load capacity. The wires of the hanging version are loaded in tension by the gravity force whereas the wires of the standing version are loaded in compression. Hence, the load-carrying capacity of the standing version is limited by buckling. Moreover, it is customary to have the workspace beneath the pick and place robot which is e.g. a conveyer belt. Thus, also from a practical perspective, the hanging version performs better than the standing version.

Another configuration is to change the orientation of topology **2DOF-2** between  $\phi_1 = 0^\circ$  and  $\phi_1 = 90^\circ$ . The shown configuration is for  $\phi_1 = 0^\circ$  which is advantageous because the T-DoF of topology **2DOF-2** (big arrow) is in the same direction as the translational components in the  $x$ -direction (smaller arrow) of the circular paths which

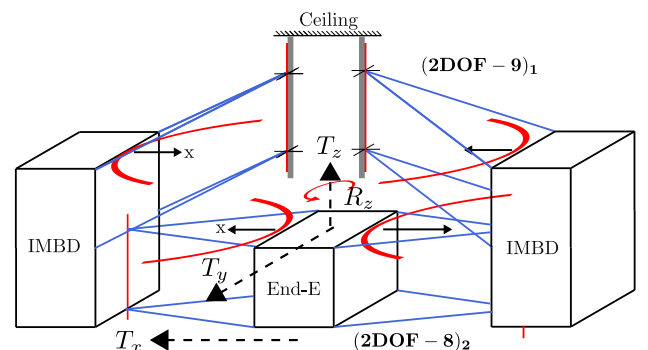


Figure 9: anipulator concepts cat. II/III: Flipped version with topologies stacked above each other.

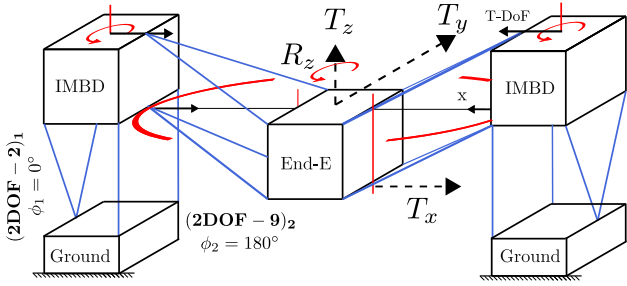


Figure 10: Manipulator concepts of cat. IV/V: Standing version, with topology **2DOF-2** oriented w.r.t. Z-axis  $\phi_1 = 0^\circ$  and  $\phi_2 = 180^\circ$ .

is introduced by bending of topology **2DOF-9**. Therefore, the IMBDs of both legs can translate inwards thus no stiffening of the manipulator occurs while moving the end-effector in the  $y$ -direction. Changing the orientation of topology **2DOF-2** to  $\phi_1 = 90^\circ$  will result in stiffening because the IMBDs can not move as it acts in the stiff direction of topology **2DOF-2**.

Therefore, the hanging configuration with  $\phi_1 = 0^\circ$ , thus the one shown in Figure 11 is the selected concept of manipulator cat. IV/V for comparison with manipulator cat. II/III.

#### 4.3.4. Selection of manipulator cat. II/III or cat. IV/V

Manipulator cat. IV/V is selected for the manipulator concept instead of manipulator cat. II/III for two reasons. First of all, the concept of manipulator cat. IV/V is approximately twice as stiff in the vertical direction as manipulator cat. II/III. The wires of topology **2DOF-2** of manipulator cat. IV/V are axially loaded in tension by gravity whereas the wires of topology **2DOF-8/9** are loaded in bending by gravity. The axial stiffness of a wire is orders of magnitude larger than its bending stiffness. The combined stiffness,  $K$ , of the leg is equal to  $K = 1/(1/K_1 + 1/K_2)$ , [15], where  $K_1$  and  $K_2$  are the stiffness of the topology connected to the ground and to the end-effector. The  $K_2$  is for both legs the same but  $K_1$  is orders of magnitude larger **2DOF-2** than the  $K_1$  of **2DOF-8/9**. Therefore, is manipulator cat. IV/V approximately twice as stiff in the vertical direction as manipulator cat. II/III.

Secondly, it is shown in paper [16], that the axial stiffness remains constant during torsional deformations whereas the axial stiffness during bending declines rapidly after deformation. Topology **2DOF-2** is deformed by torsion, hence the manipulator concept of manipulator cat. IV/V has a higher and more constant support stiffness over its ROM.

Thus, the manipulator concept of cat. IV/V is selected because it has a higher support stiffness during the ROM.

#### 4.3.5. Leg selection CLS-IV or CLS-V

For the manipulator concept, CLS-IV is selected instead of CLS-V because of its smaller size. CLS-V results

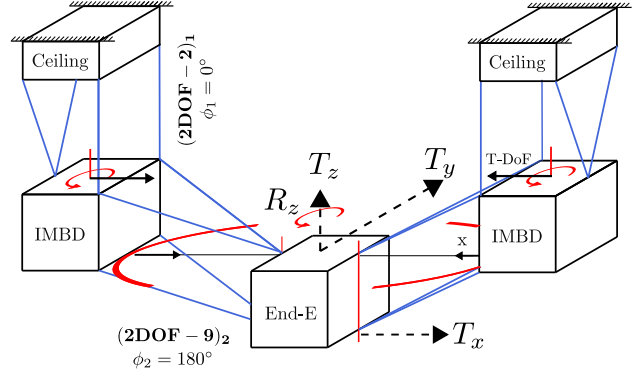


Figure 11: Manipulator concepts of cat. IV/V: Hanging version, with topology **2DOF-2** oriented w.r.t. Z-axis  $\phi_1 = \phi_2 = 0^\circ$ .

in a wider concept than CLS-IV for equal wire lengths because these of topology **2DOF-8** are oriented horizontally and these of topology **2DOF-9** are approaching the end-effector from above at an angle  $\beta$ . Hence, the end-effector of the manipulator concept CLS-IV is able to work in smaller areas e.g. within boxes.

#### 4.3.6. Finalizing manipulator concept CLS-IV

The sequence of the topologies within the CLS-IV can be varied because none of the design variables  $\mathbf{r} = (r_x, r_y, r_z)$  for the location are fixed. Connecting topology **2DOF-2** to the end-effector results in a wider and thus heavier end-effector compared to connecting topology **2DOF-9** to the end-effector. A lighter end-effector is advantageous for the operating speed of the compliant manipulator. Furthermore, a smaller end-effector is able to work in smaller areas. Hence, topology **(2DOF-2)1** is connected to the ground and **(2DOF-9)2** to the end-effector.

The rotational axis (the intersection point of the wires) of topology **(2DOF-9)2** can be placed at the end-effector or the intermediate body because its  $\phi_2$  is the last free design variable. It is decided to locate the intersection point of the wires at the end-effector as it results in a smaller end-effector.

To conclude, the selected concept for the multi-DoF compliant manipulator is a mirrored design composed of two parallel CLS-IV which are hanging at the ceiling and whose topologies are configured such as shown in Figure 11.

## 5. Experimental evaluation

The concept selection determined the theoretical layout of the demonstrator which comprises the positions and orientations of the wires, the intermediate bodies and, the end-effector w.r.t. the ground. Appendix E includes how the concept is designed and produced resulting in a physical demonstrator whereof pictures are included from different angles. The picture in Figure 12 indicates the spatial arrangement of the demonstrator comprising two legs located on the left and right side of the end-effector (grey rb).

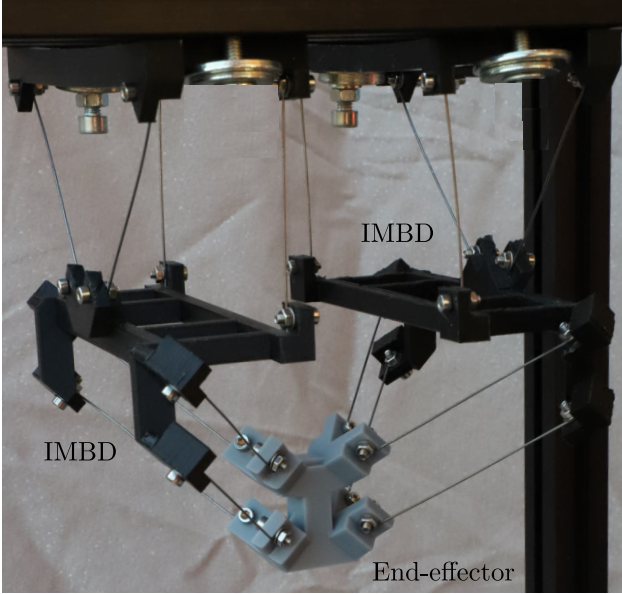


Figure 12: The demonstrator: the selected hanging manipulator concept is with two mirrored CLS-V. Topology- $(2\text{DOF} - 2)_1$  is connected to the ceiling and topology- $(2\text{DOF} - 9)_2$  to the end-effector (grey). The topologies of the CLS are connected by the black intermediate rigid body (IMBD).

Each leg is composed of one IMBD (black rb) which connects two serial compliant topologies,  $(2\text{DOF} - 2)_1$  and  $(2\text{DOF} - 9)_2$ , of which each comprising four wire flexures in parallel (slender grey parts).

This section describes the four tests which are performed as an experimental evaluation of the selected concept. The aim of each test is to qualitatively validate the theoretical principles of the COMAD-method by analyzing the displacement, the deformation and the kinematics of the demonstrator for each primary motion direction. A fishing wire is attached to the end-effector. The displacement is imposed by manually pulling the end-effector from its initial position towards one of the four primary directions respectively, until the deformation or pulling force feels disproportionate. The result is photographed from which the total displacement is determined using a grid paper (block size 5mm) behind the demonstrator. More detailed pictures are presented in Appendix E.

The results of each test is shown in Figure 13 and 14. Note, that in both figures the picture in the middle denotes the initial position included for comparison. Figure 13 presents the front view (xz-plane) of the demonstrator, with the results of the translation in the  $T_x$ -direction and  $T_z$ -direction in the upper and lower picture, respectively.

The total displacement in the  $T_x$ -direction is 2.0 cm resulting from the deflection of both  $(2\text{DOF} - 2)_1$ -topologies in their T-DOF direction. These topologies have a unit contribution because both  $(2\text{DOF} - 9)_2$ -topologies remain undeformed. Hence, the end-effector translate linearly along with the IMBDs whereby a parasitic  $T_z$ -displacement of 0.5 cm upwards is induced as a consequence of the S-

shaped bending of the  $(2\text{DOF} - 2)_1$ -topologies.

The total displacement in the  $T_z$ -direction is 2.8 cm resulting from a simultaneous deformation of all topologies in their T-DoF direction. The main contribution is provided by the deformation of the  $(2\text{DOF} - 9)_2$ -topology. Its T-DoF has an angle of  $\beta = 45^\circ$  deg with the Z-axis as it acts perpendicular to the wires thus has a component

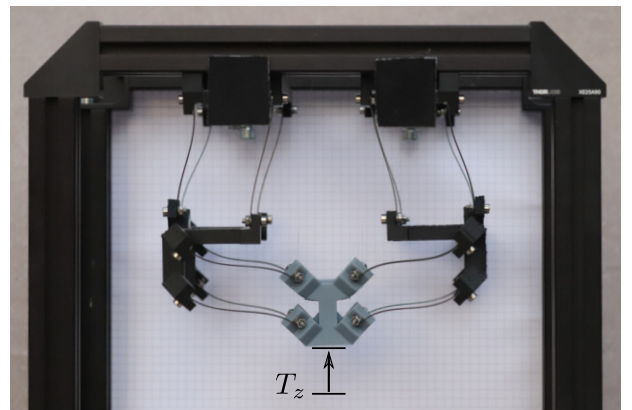
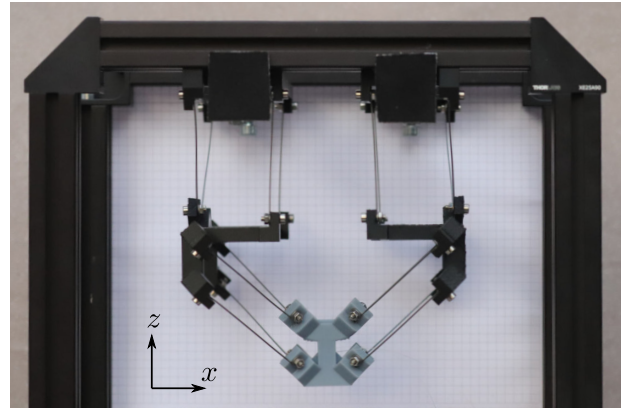
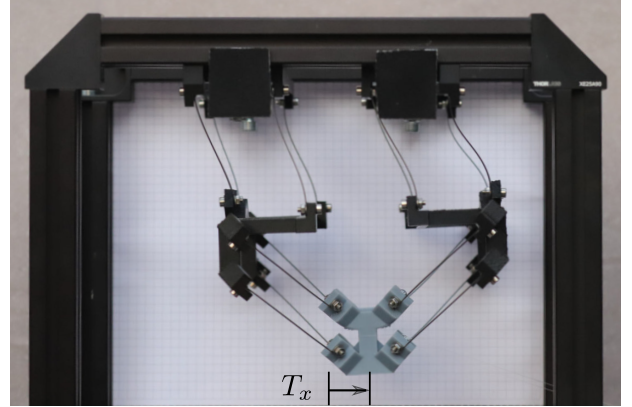


Figure 13: Front view (xz-plane) demonstrator: Upper picture: displacement in  $T_x$ -direction due to the deformation of the  $(2\text{DOF} - 2)_1$ -topology. Middle picture: denotes the initial position included for comparison. Lower picture: displacement in  $T_z$ -direction due to a deformation of the  $(2\text{DOF} - 9)_2$ -topology upwards while both IMBDs move outwards due to a deformation of the  $(2\text{DOF} - 2)_1$ -topology. This is equal to the kinematics of Figure 3.

in the  $T_x$ - and in the  $T_z$ -direction ( $\beta$  of  $(2\text{DOF} - 9)_2$ -topology in CLS-IV of Figure 4). The end-effector moves in a straight line upwards while both IMBDs move 1.2cm outwards in the T-DoF direction of  $(2\text{DOF} - 2)_1$ -topology. These kinematics are the result of the  $T_x$ -component of  $(2\text{DOF} - 9)_2$ -topology and the symmetry of the mechanism.

Figure 14 presents the bottom view ( $xy$ -plane) of the demonstrator, with the results of the translation in the  $T_y$ -direction and the rotation in the  $R_z$ -direction in the upper- and lower-picture, respectively.

The total displacement in the  $T_y$ -direction is 2.3 cm resulting from a simultaneous deformation of all topologies in their R-DoF direction. The left IMBD rotates counter-clockwise while the right IMBD rotates clockwise, both obtained by torsion of the posterior topology  $(2\text{DOF} - 2)_1$  of the picture. The end-effector moves in a straight line upwards because of the symmetry of the mechanism while bending the prosthesis topology  $(2\text{DOF} - 9)_2$ . Simultaneously, both IMBDs are slightly translating inward due to the  $T_x$ -component along the rotational path while rotating. This motion is obtained by the deformation of the topology  $(2\text{DOF} - 2)_1$  in its T-DoF direction.

The total rotation of the end-effector is  $18^\circ$  resulting from a simultaneous deformation of all topologies in their R-DoF direction. The rotational motion is obtained by pulling the left and right sides of the end-effector. Both topologies of the right leg and the  $(2\text{DOF} - 2)_1$  topology of the left leg rotate along with the end-effector while the left posterior topology  $(2\text{DOF} - 2)_1$  rotates in an opposite direction. The angle of rotation of the left topology is larger than the right  $(2\text{DOF} - 2)_1$  topology.

As a fifth and a sixth test, a moment is imposed at the end-effector around the  $R_x$ - or the  $R_y$ -axis resulting in no displacements by the presence of a significant constraint stiffness.

As a total result of the experimental evaluation has the COMAD-demonstrator performed four decoupled motions in the primary  $(T_x T_y T_z R_z)$  directions with values as is presented in Table 4. Furthermore the demonstrator constrains the motion around the  $R_x$  and  $R_y$ -axes. The observed topology deflections are equal to the kinematics of the rb-parallel mechanism of Figure 3. The T-DoF and R-DoF of the  $(2\text{DOF} - 2)_1$  topology correspond to the  $T_1$  and  $R_1$  DoF of Figure 3, and the T-DoF and R-DoF of the  $(2\text{DOF} - 9)_2$  topology correspond to the  $T_2$  and  $R_2$  DoF. So, the motion pattern is as required and obtained by the

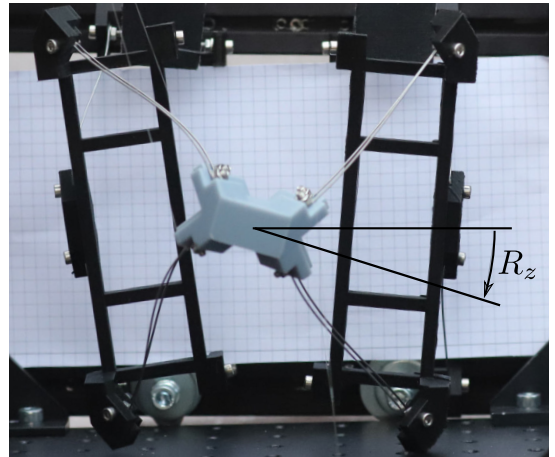
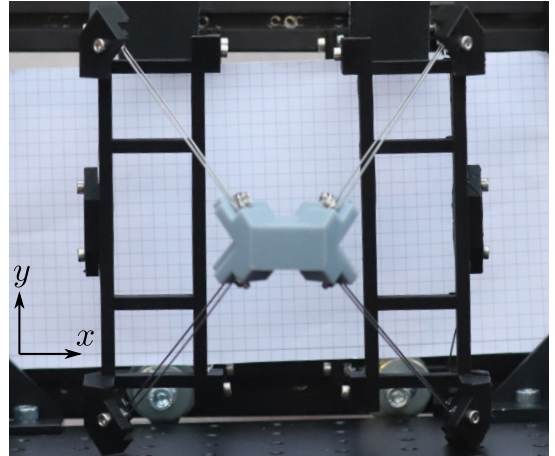
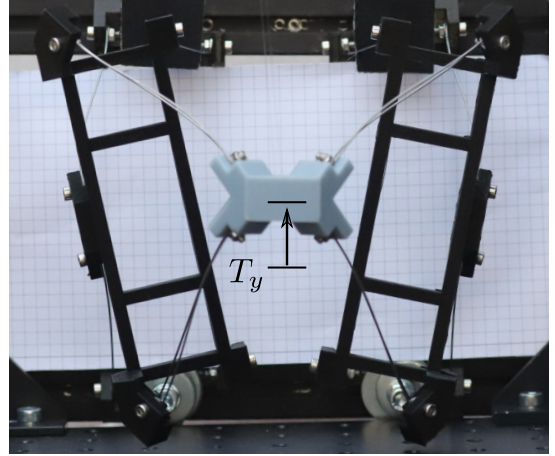


Table 4: Test results: displacement per primary motion direction of the demonstrator.

Test direction			
$T_x$	$T_y$	$T_z$	$R_z$
2.0 cm	2.3 cm	2.8 cm	$18^\circ$

Figure 14: Bottom view ( $xy$ -plane) demonstrator: Upper picture: displacement in  $T_y$ -direction due to the counter-rotation of both IMBDs while deforming the (posterior)  $(2\text{DOF} - 2)_1$ -topology and the (prosthesis)  $(2\text{DOF} - 9)_2$ -topology by respectively, torsion and bending. Middle picture: denotes the initial position included for comparison. Lower picture: rotation around  $R_z$ -axis due to a counter-clockwise rotation of the left IMBD while the right IMBD rotates clockwise, both obtained by torsion and bending of the  $(2\text{DOF} - 2)_1$ - and  $(2\text{DOF} - 9)_2$ -topology.

simultaneous deformations of the flexible wires originating from the parallel kinematic coupled relations.

Although the intention of the test was purely qualitative, the first results of the achieved motions are significant, 2.0-2.8cm and  $18^\circ$ , w.r.t. to the size of the demonstrator (145x170x170)mm and as compared to the compliant mechanism presented in, "A 2-DOF large stroke flexure based positioning mechanism" [17], of which it is known that it has a relatively large workspace-area to footprint ratio (1/32). This comparison is only a conservative indication of the achieved values during this test because the mechanism of [17] is further developed and its performance was measured using the first eigenfrequency which has to remain larger than 100 Hz which has limited the ROM.

However, the achieved displacements can be seen as a direct result of the coupled relations because, as observed, the total displacement in the  $T_y$ ,  $T_z$ - and  $R_z$ -direction benefit from the simultaneous deformation of all topologies. For example, the ROM in the  $T_y$ -direction can only be obtained while both IMBDs are moving outwards, else, nonlinear stiffening of the demonstrator occurs. Thus, although the  $(2\text{DOF} - 2)_1$ -topology is not deflected in the  $T_z$ -direction, it positively influences the mechanics of the manipulator.

## 6. Discussion and Recommendation

This section will discuss the two main findings during this research. The first one is that the spatial ROM of parallel legged compliant manipulators is larger compared to serial compliant manipulators. The second finding is that the architectures of these spatial parallel concepts are mainly dominated by wires flexures.

### 6.1. Range of Motion

Three explanations can be associated with the finding that the ROM of parallel compliant manipulators is larger than serial compliant mechanisms. This was an unexpected because for rb-mechanisms the contrary generally holds, namely, the ROM of an rb-parallel mechanism is usually smaller than the ROM of an rb-serial mechanism.

The first explanation for the enlarged ROM is that the total displacement of a parallel compliant mechanism has an added contribution of two deflecting compliant topologies in series (e.g. CLS II-V) while a serial compliant mechanism has a unit contribution of one deflecting compliant topology (e.g. CLS I). This added contribution is directly related to the parallel coupled relations whereas the unit contribution is typical for serial mechanisms, such as shown in Figure 2 and 3. The maximal deflection of a single flexure is limited by exceeding the elastic regime, thus the added contribution to the deflection of a parallel compliant mechanism results in an enlarged ROM.

Rb-joints have an approximately infinite ROM and therefore the ROM of a rb-mechanism is generally limited by

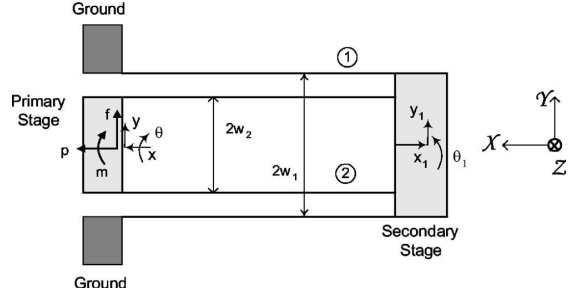


Figure 15: Compliant mechanisms obtained by a serial kinematic solution and composed of identical serial stacked modules with parallel arranged flexures. The mechanism has an uncontrolled intermediate body (IMBD) due to the present of a redundant T-DoF. Figure obtained from [18].

the global kinematics which causes the difference in result. An example of a global limit is a singular point or the moment when the links of a leg are fully aligned, such as presented in Appendix A.

The second explanation is an improved constraint stiffness behavior during motion because the IMBD of a parallel compliant mechanism is controlled by its kinematics. This enlarges the ROM because it is limited when the stiffness in the constraint direction becomes insufficient as a consequence of flexure deformation. The influence of an (un)controlled IMBD on the stiffness is explained in the paper "Characteristics of beam-based flexure modules" of Awtar et. al. [18] by comparing two mechanisms composed of two serially stacked modules both having a 1-DoF translational motion. The first compliant mechanism is shown in Figure 15 and has an uncontrolled IMBD because it possesses the same T-DOF as the end-effector, meaning that this DoF is redundant [13]. Therefore, the IMBD is underconstrained and thus free to move even when the end-effector is held fixed. This results in a rapidly decreasing vertical constraint stiffness when the mechanism is moved out of its initial position [18].

The second compliant mechanism [18] is shown in Figure 16 and is obtained by a parallel kinematic solution because its translational motion is dependent on a simultaneous rotation  $\theta$  of the two R-DoF of the leg. The mech-

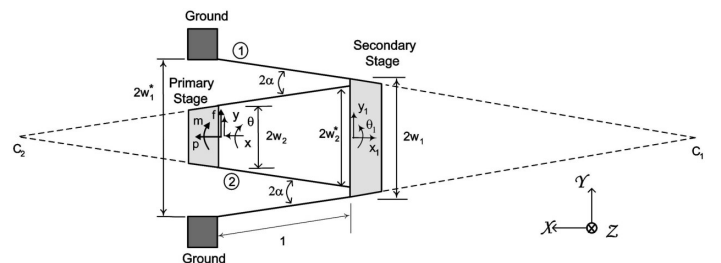


Figure 16: Compliant mechanisms obtained by a parallel kinematic solution and composed of identical serial stacked modules with tilted arranged flexures. The mechanism has a controlled intermediate body (IMBD) because the translation and the rotation is kinematically related to the translation and rotation of the end-effector. Figure obtained from [18].

anism in Figure 16 has a controlled IMBD because its angle  $\theta$  is related to its position  $T_y$ , and is therefore, kinematically dependent on the translational position of the end-effector. Therefore, the IMBD cannot move independently from the end-effector which result in a better stiffness in the constraint direction during motion[18].

There are similar kinematics observed between compliant manipulator concepts II-V, the mechanism of Figure 16, and the PM in Figure 3 because for all these three mechanisms is the motion in the  $T_y$ -direction depending on coupled relations between the two R-DoFs of their leg.

Lastly, the experimental evaluation of the demonstrator confirms that parallel compliant mechanisms have a larger ROM. Although the demonstrator is a parallel mechanism, it is suitable to compare a serial related motion, such as the  $T_x$ -motion, with motions obtained by parallel coupled relations, the  $T_y$ -,  $T_z$ - and  $R_z$ - motion. Comparing the deformations and tangible stiffness in these directions, two findings contribute to a larger ROM.

First, the maximal flexure formation is smaller towards the  $T_y$ -,  $T_z$ -directions than towards the  $T_x$ -direction, while the displacements are slightly larger (with a factor 1.15-1.40 w.r.t.  $T_x$ -), as seen in Figure 13 and Figure 14. The flexures at the top right of Figure 13 show a large S-shaped deformation because the motion in  $T_x$  -direction is solely obtained by topology **2-DOF2** while the bottom part of the mechanisms remains undeformed. The motion in the  $T_y$ - and  $T_z$ -direction is obtained by the deformation of both topologies. As seen, this results in an equal deformation per topology which therefore remains smaller.

Secondly, the tangible stiffness remains relatively constant in the actuation direction of the  $T_y$ - and  $T_z$ -direction while the stiffness development is rapidly increasing in the actuation direction of the  $T_x$ -motion. The bending angle of the wires in the  $T_x$ -direction is larger and, therefore, the motion direction is more aligned with its axial direction which results in an increasing contribution of the axial stiffness during motion. So, this test quantitatively confirmed that the ROM benefits from the parallel coupled relations as the flexure deformations remain smaller for comparable displacements. In order to quantify the ROM of a parallel and serial multi-DoF compliant manipulators in general, a test ought to be performed which determines the difference in maximal displacement while remaining within an acceptable limit for internal material stress and (measurable) stiffness characteristics in actuation and constraint directions and within proportional limits compared to the deformations in the  $T_x$ -direction.

## 6.2. Wire flexures

Wire flexures are dominating the architectures of parallel compliant manipulators which is a remarkable finding because generally leaf springs are used within compliant mechanism designs. However, a leaf spring adds relatively much (three planar) constraints to a parallel compliant manipulator which requires multiple axes flexibility. This

flexibility is necessary to obtain the parallel coupled relations within a firmly united design. Moreover, a leaf spring is too spacious for compliant manipulator designs because they are limiting the placement options for other constraint elements without intersections. Thus, despite that a leaf-spring is used in e.g. compliant joints or planar multi-DoF mechanisms, wires are beneficial to use within compact multi-DoF spatial compliant manipulators.

A wire can be orientated such that the freedom of a body is precisely constraint along one specific direction while there is still space to add other wires. Wires afford a multi-functionality to deform in all required kinematically coupled directions. Therefore, combining differently arranged wire flexures provide the ability to integrate multi-DoF parallel compliant manipulators within one flexure system while the spatial motion pattern remains. However, designing compliant manipulators composed of wires requires some caution because they are very sensitive to buckling when loaded in compression. Therefore, hanging designs such as the current design in this article Figure 11, are beneficial as its wires can be loaded in tension.

For future research, it is interesting to investigate the actuation of a multi-DoF compliant system comprising flexible wires that provide the motion. The demonstrator of this article provides the permissible the motions and necessary constraints directions for the manipulator. However, actuation has to be added to become a functional manipulator for the industry. Actuation through the wires could be challenging because it has 5-DoF and a distributed compliance along its length. In comparison, revolute and prismatic rb-joints permit motion in 1-DoF which in turn facilitates actuation by common actuators such as electric rotary- or linear actuators each applying 1 R-DoF or 1 T-DoF, respectively. Physically connecting a 1-DoF rotary- or linear actuator directly to the wire is difficult because the actuator will deform the wire during its motion. Four actuation concepts will be discussed which would be interesting to investigate in further research

The first concept is that the wire could be actuated at a sliding point to prevent a physical connection which has to deform along with the wire. However, hardly any motion will be transferred to the end-effector because the wire will deform locally and remain undeformed at its ends. The second concept is a deformable sub-mechanism which transfer the actuation along the length of wire and to deform along with the wire. However, the deformable sub-mechanism has to be multi-DoF because the wire must be able to deform in multiple directions as a consequence of the parallel kinematic relations. However, multi-DoF deformable mechanisms might be designed with the COMAD-method as they are compliant mechanisms but it will add complexity to the manipulator.

The third actuation concept is that the actuators are placed between the ground and the IMBDs or placed between the IMBDs of both legs. An rb hinge or deformable sub-mechanism is needed to transfer the motion when the rigid bodies are moving. A deformable sub-mechanism

which transfers the actuation between two rigid points with 2-DoF that are predictable is less complex compared to a flexible wire. However, friction, backlash, wear and lubrication of these 1-DoF actuators are presented thus limiting the precision of the compliant manipulator.

The fourth concept is to actuate without a mechanical connection between the manipulator and the actuator. For example, electromagnetic components which are placed upon the end-effector or IMBDs. These components could be attracted or repelled by electromagnets which are placed within a reachable distance of the manipulator. The applied Lorenz force upon the end-effector or IMBDs deforms the flexible wires. The deformation will be large in the compliant directions of the mechanism and small in its stiff directions. The end-effector could be moved in its primary motion directions because the multi-DoF compliant manipulator guides this motion. Altogether, it would be interesting for future research to investigate the potentials of electromagnetic actuation for multi-DoF compliant manipulators composed of flexible wires, to result in a movable manipulator.

## 7. Conclusion

The COMAD-method was presented in this paper, which was shown to be an effective procedure for designing spatial multi-DoF compliant manipulators as it offers a variety of new concepts. The uniqueness of the method is the incorporation of parallel kinematics solutions by performing the "Type synthesis of legs", after which the compliant concepts are obtained using the FACT-method.

In this article, a 4-DoF compliant demonstrator with a spatial TTTR-motion pattern was developed build and tested and successfully showing four decoupled motions. These motions were obtained by a simultaneous deformation of all compliant topologies. This results in a summed displacement of the serial topologies and improved stiffness properties by a kinematically controlled intermediate body. The parallel coupled relations are responsible for these two effects, however, how it influences the motion characteristics of parallel compliant mechanisms in general ought to be quantified in further research.

The selected concept for the demonstrator is one of the four new obtained mechanisms. These mechanisms were shown more compact and permitting a larger ROM compared to those obtained from conventional methods. The resulting demonstrator can be seen as a new milestone as it solves the current problems of compliant manipulators within the e.g. high-tech industry.

## 8. References

### References

[1] I. F. of Robotics, "Robots double worldwide by 2020," <https://ifr.org/ifr-press-releases/news/robots-double-worldwide-by-2020>, 2018, accessed: 2019-11-07.

[2] R. I. Association, "Pick and place robots: What are they used for and how do they benefit manufacturers," <https://www.robotics.org/blog-article.cfm/Pick-and-Place-Robots-What-Are-They-Used-For-and-How-Do-They-Benefit-Manufacturers/88>, 2018, accessed: 2019-11-07.

[3] X. Kong and C. M. Gosselin, *Type synthesis of parallel mechanisms*. Springer, 2007, vol. 33.

[4] B. Siciliano and O. Khatib, *Springer handbook of robotics*. Springer, 2016.

[5] L. L. Howell, *Compliant mechanisms*. John Wiley & Sons, 2001.

[6] L. L. Howell, S. P. Magleby, B. M. Olsen, and J. Wiley, *Handbook of compliant mechanisms*. Wiley Online Library, 2013.

[7] S. Henein, P. Spanoudakis, S. Droz, L. I. Myklebust, and E. Onillon, "Flexure pivot for aerospace mechanisms," in *10th European Space Mechanisms and Tribology Symposium, San Sebastian, Spain*, 2003, pp. 285–288.

[8] S. T. Smith, *Flexures: elements of elastic mechanisms*. CRC Press, 2014.

[9] M. Berglund, S. Magleby, and L. Howell, "Design rules for selecting and designing compliant mechanisms for rigid-body replacement synthesis," in *Proceedings of the 26th Design Automation Conference, ASME DETC, Baltimore, MD*, vol. 14225, 2000.

[10] M. Pucheta and A. Cardona, "Kinematics synthesis of compliant mechanisms using rigid-body replacement," *Multibody Dynamics*, pp. 156–157, 2007.

[11] J. B. Hopkins and M. L. Culpepper, "Synthesis of multi-degree of freedom, parallel flexure system concepts via freedom and constraint topology (fact)—part i: Principles," *Precision Engineering*, vol. 34, no. 2, pp. 259–270, 2010.

[12] —, "Synthesis of multi-degree of freedom, parallel flexure system concepts via freedom and constraint topology (fact). part ii: Practice," *Precision Engineering*, vol. 34, no. 2, pp. 271–278, 2010.

[13] —, "Synthesis of precision serial flexure systems using freedom and constraint topologies (fact)," *Precision Engineering*, vol. 35, no. 4, pp. 638–649, 2011.

[14] G. Hao, H. Li, X. He, and X. Kong, "Conceptual design of compliant translational joints for high-precision applications," *Frontiers of Mechanical Engineering*, vol. 9, no. 4, pp. 331–343, 2014.

[15] H. Soemers, *Design Principles for precision mechanisms*. T-Pointprint, 2011.

[16] D. Wiersma, S. Boer, R. G. Aarts, and D. M. Brouwer, "Design and performance optimization of large stroke spatial flexures," *Journal of computational and nonlinear dynamics*, vol. 9, no. 1, p. 011016, 2014.

[17] K. Folkersma, S. Boer, D. Brouwer, J. Herder, and H. Soemers, "A 2-dof large stroke flexure based positioning mechanism," in *ASME 2012 International Design Engineering Technical Conferences and Computers and Information in Engineering Conference*. American Society of Mechanical Engineers Digital Collection, 2012, pp. 221–228.

[18] S. Awtar, A. H. Slocum, and E. Sevincer, "Characteristics of beam-based flexure modules," *Journal of Mechanical Design*, vol. 129, no. 6, pp. 625–639, 2007.

[19] W. Wittrick, "The theory of symmetrical crossed flexure pivots," *Australian Journal of Chemistry*, vol. 1, no. 2, pp. 121–134, 1948.

[20] B. D. Jensen and L. L. Howell, "The modeling of cross-axis flexural pivots," *Mechanism and machine theory*, vol. 37, no. 5, pp. 461–476, 2002.

[21] Z. Hongzhe and B. Shusheng, "Accuracy characteristics of the generalized cross-spring pivot," *Mechanism and Machine Theory*, vol. 45, no. 10, pp. 1434–1448, 2010.

[22] B. P. Trease, Y.-M. Moon, and S. Kota, "Design of large-displacement compliant joints," *Journal of mechanical design*, vol. 127, no. 4, pp. 788–798, 2005.

[23] B. Shusheng, Z. Hongzhe, and Y. Jingjun, "Modeling of a

- cartwheel flexural pivot," *Journal of mechanical design*, vol. 131, no. 6, p. 061010, 2009.
- [24] S. Zelenika and F. De Bona, "Analytical and experimental characterisation of high-precision flexural pivots subjected to lateral loads," *Precision Engineering*, vol. 26, no. 4, pp. 381–388, 2002.
- [25] X. Pei, J. Yu, G. Zong, S. Bi, and H. Su, "The modeling of cartwheel flexural hinges," *Mechanism and Machine Theory*, vol. 44, no. 10, pp. 1900–1909, 2009.
- [26] D. M. Brouwer, J. P. Meijaard, and J. B. Jonker, "Large deflection stiffness analysis of parallel prismatic leaf-spring flexures," *Precision engineering*, vol. 37, no. 3, pp. 505–521, 2013.
- [27] L. Lamport, *A Document Preparation System*, 2nd ed. Addison-Wesley, 1994, user's Guide and Reference Manual.

## Discussion and conclusion

The COMAD-method can be considered as an enrichment for designing multi-DoF compliant manipulators, resulting in new solutions that are not likely to be found with other methods. The potential of other multi-DoF designs which were not obtained in the compliant solutions space of the treated design case are discussed first in this chapter. Subsequently, the general applicability of the newly obtained multi-DoF mechanisms is discussed with two concepts of applications to gripper designs and an example of an application for a spatial positioning stage with a high precision.

### 3-1 Potential of unexplored designs

Using the COMAD-method for the presented design case has resulted in four additional compliant solutions (CLS II-V) compared to the FACT-method by which exclusively compliant solution CLS-I would have been obtained, which listed in Chapter 2.3 and shown in Figure 4. However, the compliant solution space was limited by two reasons, first solely 4-DoF legtypes are considered as kinematic solutions and second, solely compliant solutions are obtained composed of  $n = 2$  serial topologies. The kinematic solution space could be expanded by four additional 5-DoF legtypes,  $\mathcal{T}_{leg-5}$ : **3T2R**, **2T3R**, **1T4R**, **5R** [9]. Additionally, the compliant solution space will be even larger when if also flexure systems composed of  $n \leq 3$  topologies are included. It was established in Chapter 2 that the translational motion of the compliant mechanism benefits from the inherent kinematic couplings between multiple R-DoF within its legs. In addition it is also established that the total displacement of a parallel compliant mechanism is enlarged by the deflection of multiple topologies in series. The unexplored design potentially permits large ROM due to these two advantages. Therefore, it is interesting for further research to investigate the ROM capabilities of these unexplored designs which are obtained by legtypes whose set-of-DoF comprises three or more R-DoF (e.g. 4-DoF-legtype-3,  $\mathcal{T}_{leg,3} = \mathbf{1T3R}$ , or by 5-DoF-legtype,  $\mathcal{T}_{leg-5} = \mathbf{2T3R}$ ). It is expected that the translational motion in the Tx- and Ty-direction of these manipulator designs will be obtained by multiple counter rotating R-DoF. This potentially enlarges the translational ROM in the x-direction because half of the current demonstrator is not deforming during motion in its Tx-direction as it is obtained by a unit contribution of the T-DoF of the legtype-2,  $\mathcal{T}_{leg,2} = \mathbf{2T2R}$ . It is also expected that an additional IMBD and a third  $n = 3$  serial compliant topology is necessary for legtypes whose set-of-DoF comprises three R-DoF. A finding during this research was namely that the number  $n$  of serial compliant topologies must be equal to the number of R-DoF of the legtype as a consequence of geometric condition-1 that requires that all R-axis must be aligned R-axes in parallel. The use of a third serial R-DoF leads in turn also to a potential increase of the ROM because the total displacement in both Ty- and Tx- direction will be the result of three added deflections in series.

Due to the increase in the number of serial topologies, it is interesting for further research to minimize the volume of the obtained mechanisms. This possible because they are composed of thin wire flexures

which can be nested and crisscrossed among each other. As an example, Figure 3-1 presents the current (deployed) design of the demonstrator but it can be more compactly aggregated by folding the topologies of the legs through each other. Such a folded version is presented in Figure 3-2 and obtained by rotating topology **2DOF-2** and the IMBD with  $180^\circ$  while topology **2DOF-9** and the end-effector retain their original orientation. The resulting volume of the compact mechanisms is half of the deployed mechanism. Therefore, the addition of a third topology does not necessarily result in a significant increase in the mechanisms volume.

Thus the ROM capabilities of the unexplored concepts are interesting for further research because in two directions is their translational motion obtained by parallel kinematic relations between three deflecting topologies while the volume could remain the same.

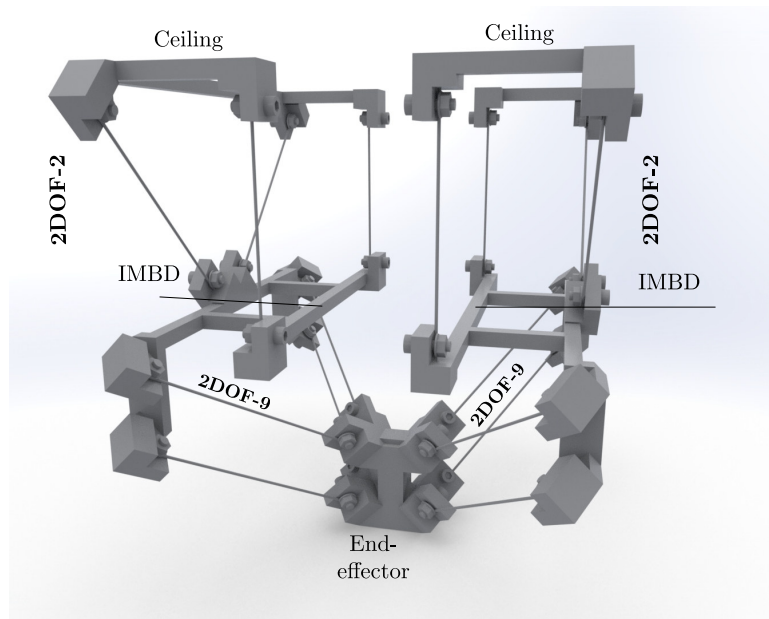


**Figure 3-1:** The current demonstrator. Deployed leg; topology **2DOF-2** is aligned above topology **2DOF-9**. The mechanisms is fixed at the ceiling.

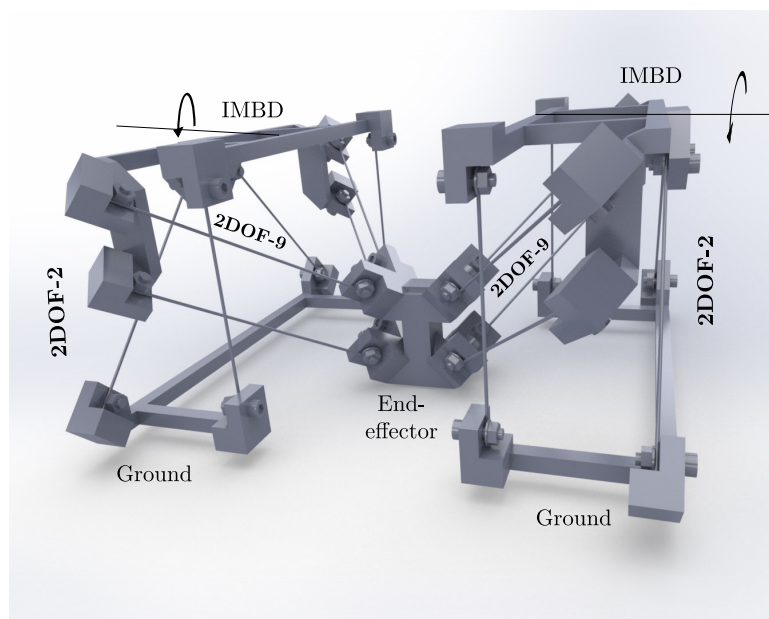


**Figure 3-2:** The folded version of demonstrator which is more compactly aggregated by rotating topology **2DOF-2** and the IMBD with  $180^\circ$  while topology **2DOF-9** and the end-effector retain their original orientation. By folding the leg reduces half of the volume w.r.t. Figure 3-1) because the wires are nested and crisscrossed among each other. The mechanism is fixed at the ground.

## 3-2 Applications to gripper designs

The compliant concepts of this thesis could be implemented as grippers within the food industry since grippers have to be hygienic, compact and able to deform among the uniquely shaped, delicate and deformable surface of the object to distribute the pressure along its surface during the fixed grasp. Two gripper concepts that might be interesting for further research are explained.

The first gripper concept is based on touching the object using multiple end-effectors. The gripper could be composed of multiple compliant concepts that encircle the object and grasp it by moving the end-effectors towards the object. The multi-DoF functionality of the end-effector is able to approach the surface of the object and subsequently deform along with its geometrical shape while touching it. This will distribute the pressure of the gripper. The end-effectors with a higher order motion patterns, for example the  $3T2R$ - or the  $2T3R$ -motion pattern, could be synthesized using the "synthesis of leg types" in order to deform along with all 3 dimension of the curved surface.

The second gripper concept is based on touching the objects with the side or the ends of the legs such that they are used as multi-DoF gripper fingers. In such a design the R-axes of the legs are perpendicular to the surface of the object in order to have the compliant direction normal to the objects surface. Instead of touching the object with the end-effector (top of the finger) itself, it will be actuated by a robotic arm and displaced towards the middle of the object. The legs are moving in front of the end-effector and could move around the object and touch it with the sides of the mechanisms legs, for example the legs of the concept represented in Figure 3-1 or Figure 3-2. The R-DoFs of the leg are kinematically coupled to each other; hence, all topologies will deflect along with the object. The shared deformation will distribute the pressure along the surface instead of one pressure point. The best CLS concept will be selected based on its motion behavior but also based on the less harmful geometrical layout of the side of the leg. Additional redundant wires could be selected at the side of the leg which touches the object in order to decrease the pressure spots.

## 3-3 General multi-DoF compliant mechanism applications

The COMAD-method is capable to synthesize a wide variety of multi-DoF compliant solutions for desired motion patterns in general. The resulting serial set of compliant topologies can be positioned differently resulting in different concept configurations each having specific ROM and stiffness characteristics. For each multi-DoF application are different ROM and stiffness characteristics required. For example, the manipulator concept of Figure 8 in the presented article has straight legs and larger motions result in stiffening of the mechanism hence, performs bad as pick- and place manipulator. However, this concept is suitable within applications that require a high horizontal and vertical stiffness, for example, to position an object (chip e.g.) with high precision within the focal point of a laser. Such an application requires the same motion pattern as the presented design case thus the same five CLSs concepts as in Figure 4 would be synthesized. However, the resulting kinematic behavior of the concept is strongly depended by the configuration of the synthesized topologies which are decisions of the engineer.

## 3-4 Conclusion

All in all, the COMAD-method can be considered as an enrichment for designing multi-DoF compliant manipulators, resulting in a variety of new solutions. The engineer is able to make a well-founded concept selection for its intended multi-DoF application because, when the engineer uses the COMAD-method, the concept is selected based upon the complete compliant solutions space. The concepts which are obtained by parallel kinematic solutions could be configured such that they have a large ROM and better stiffness capabilities compared to concepts obtained using state-of-the-art methods. Hence, this new method can be seen as a milestone in designing multi-DoF compliant manipulators as their current limitations are reduced.



## Range of motion of a parallel mechanism with one, two and three legs

In order to provide insight into the workings principles of the "type synthesis of leg" a TTTR-parallel manipulator is build using the K'nex toy and obtained by using legtype-2 = 2T2R. An example with two legs is shown in Figure A-4 and a schematic drawing in Figure A-1. The leg comprises (in sequence starting at the ground) one prismatic slider  $P_1$  in the x-direction, one prismatic slider  $P_2$  (blue arrows in Figure A-1) in the zy-direction by which the first revolute joint (red point) is attached which is connected to the revolute joint at the end-effector by one rigid link. The two revolute joints parallel aligned with the z-axis.

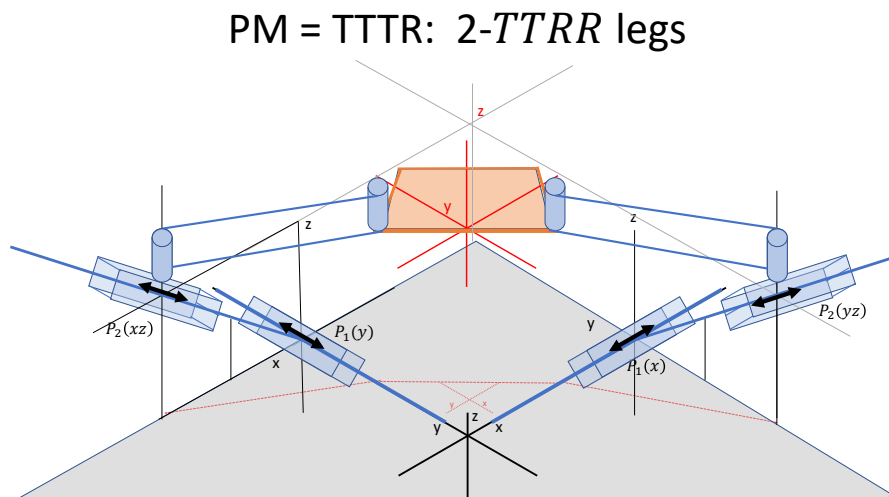


**Figure A-1:** Schematic drawing of K'nex toys model with two legs connected perpendicular to each other. The leg comprises the following four joints, starting at the ground: first slider  $P_1$  in xy plane, second slider  $P_2$  has a component in z-direction, followed by a two revolute joints connecting to the end-effector. In between a rigid link.

The effect of the number (1, 2 or 3) of parallel legs is investigated in the second test. The range of the motion of the end-effector will be compared between the three mechanisms even as the range of the strokes achieved by the four joints in the leg. Top view of the three rigid body mechanisms are presented in each row of Figure A-3. The rotational stroke of both revolute joints of the left leg is depicted in the left column, the translational stroke of the limiting slider is depicted in the right column. The effective lengths of the rotational strokes are presented as a (part of) a red circular path and of the slider as a blue arrow.

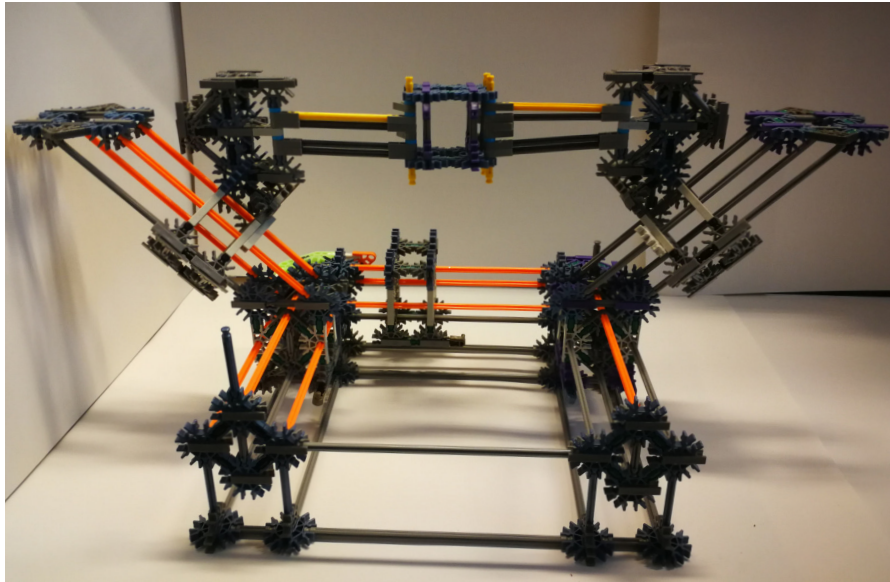


**Figure A-2:** Front view of parallel mechanism with 2 legs at its physical limit point when the legs are fully aligned. The joints of the legs corresponds to the one in Figure :SpatialTTTR but the legs are this time orientated mirrored w.r.t. each other

In the upper row of Figure A-3 is the motion of one single leg displaced. It is a rigid body serial mechanism as it comprises one leg. During the test, the ROM of the end-effector is only limited by reaching the end of a stroke of a slider. For example, it can freely move up and down along the horizontal and vertical slider of the leg. The end effector can freely rotate around the revolute joint located at the slider resulting in a circular path (two positions are shown in the top two figures). The end-effector is also able to rotate around the axis through its own body, created by the second revolute joint. Thus the range of motion of the serial mechanism is solely limited by the slider's lengths and the radius (rigid link at the end-effector) of rotation.

In the middle row of Figure A-3 is a parallel mechanism depicted with two parallel legs with a mirrored orientation w.r.t. each other. The rotational stroke of the revolute joints at the (right) legs is limited at the moment when at the other (left) rigid link plus the end-effector are aligned and thus reaching their longest length. The position of the linkage at this limit point is shown above the left mechanism. The same holds for the horizontal slider, its stroke is limited at the moment when both rigid links and the end effector are aligned, this pose of the linkage is shown above the right mechanism. The vertical slider can use the full stroke length.

In the lower row of Figure A-3, the same parallel mechanism is depicted as above but now with an additional third leg at a third side of the end-effector. The rotational stroke of the revolute joints at the (right) leg will not reach the previous limit point (mid-row) anymore because it is already limited when the end-effector and the rigid link of the third leg became in an aligned position. This position is shown on the right side of the left picture of the lower row. Also, the range of motion of the vertical slider is limited due to the addition of the third leg. The corresponding position of the linkage is shown on the left side of the right picture in the lower row. Comparing a mechanisms with two and three legs shows the same result. In Figure A-4 is in the left picture has 3 attached legs at an limit point. In the right picture is the third leg is decoupled which enlarges the ROM in the left downwards direction (blue arrow).

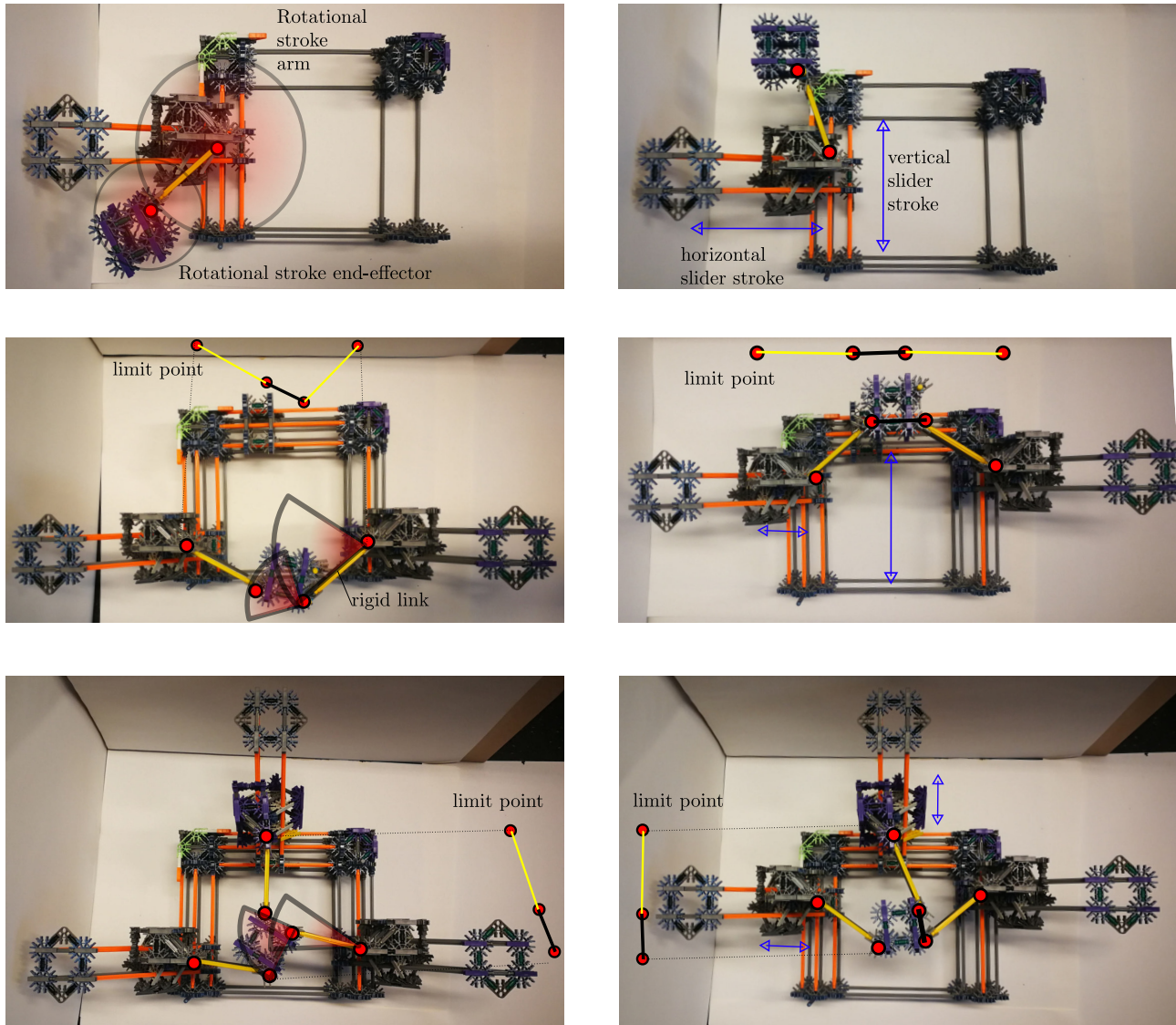


**Figure A-3:** Range of Motion (ROM) of 1 and 2 and 3 legged Mechanism. The leg comprises 2P2R. The rotational ROM is depicted in the left column (red circular path) and the translational ROM at the right column (blue line is the slider stroke reached). 1 legged Serial Mechanism (top) has the largest ROM but a different motion pattern and only limited by the stroke length of the sliders. The 2 and 3 legged parallel mechanisms (middle and bottom row) are physically limited when the linkages are aligned by moving both prismatic joints move outwards. The 2 legged mechanism has a large ROM than the 3 legged mechanism.

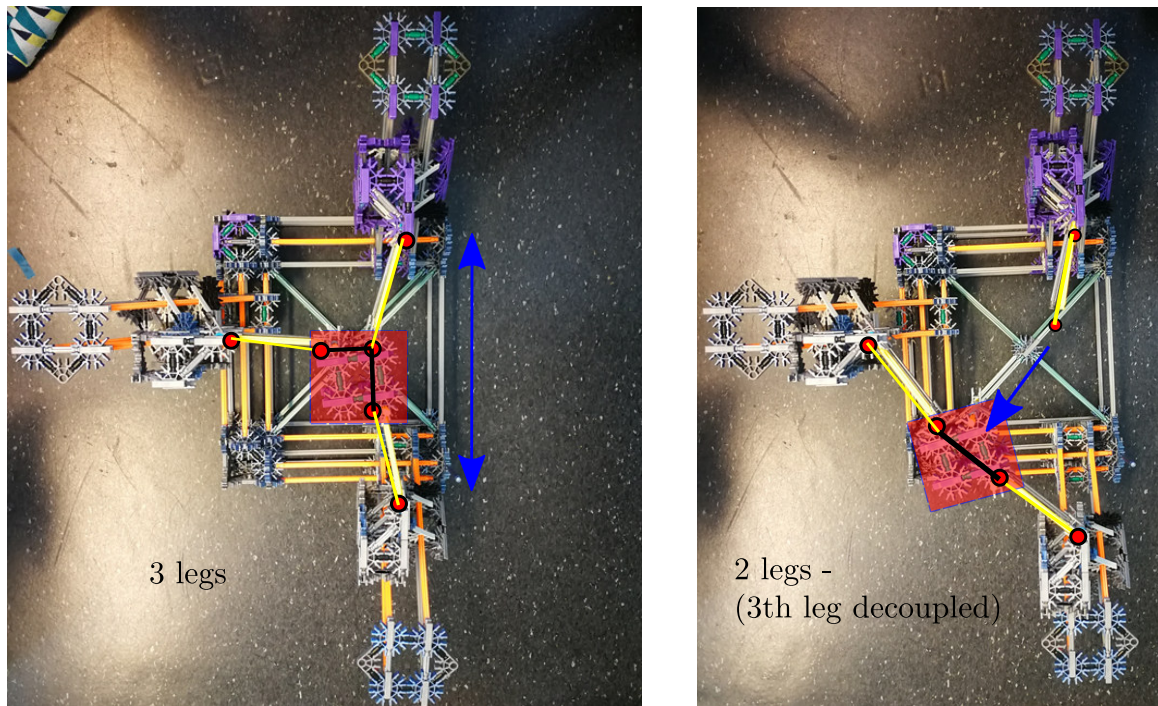


**Figure A-4:** Range of Motion (ROM), left picture has 3 attached legs at an limit point. In the right picture is the third leg decoupled which enlarges the ROM in the left downwards direction (blue arrow).

Analyzing the ROM in Figure A-3 already shows that the addition of the third leg limits the ROM. This result is confirmed in Figure A-4 as the left picture shows a mechanisms with three legs in its limit point and on the right a picture after releasing the third leg which enlarges the ROM of the end-effector towards the left bottom (blue arrow).

All in all, has the serial mechanism the largest ROM because the rotational motion of the revolute joints is infinite thus determined by the radius (rigid link length) and the translational motion is limited by the length of the slider. The rotational motion of the parallel mechanisms with two mirrored legs is limited at the moment when the end effector and the opposite leg are aligned such as was shown on the left column of Figure A-4. The translational motion of both angled sliders  $P_2$  is limited when both rigid links and the end-effector are aligned such as was shown in the right column of Figure A-4 and Figure A-3 . The addition a third parallel leg has reduced the rotational- and vertical translational ROM, because the third leg will obtain an aligned position with the end-effector in at an earlier stage.

# Effect of geometrical conditions

In order to provide insight into the workings principles of the "type synthesis of leg" a view tests are done to evaluate the influence of the geometrical conditions that must be satisfied by the legtypes. For the test a TTTR-parallel mechanism is used that comprises two parallel legtype-2 2T2R and build with the K'nex toys. The geometrical condition for the 4-DoF legtypes are as follows:

- G1) The axes of all R-DoF are always parallel.
- G2) The direction of at least one T-DoF is not perpendicular to the axes of the R-DoF.

### B-1 Geometrical condition-1

In this subsection the effect of satisfying and not satisfying will be investigated with a rb-mechanism. Each leg of the mechanisms shown in Figure B-1 is having 2 legs each contains two R-axis. The top row contains two mechanisms of which the parallel axes are non-parallel and the bottom row contains two mechanisms of which the axes are parallel. The left column is added to show the orientation of the R-axis before the end-effector is connected between the legs. As can be seen in the top left picture, are the R-axes under an angle of thirty degrees, and in the lower left picture are the R-axes parallel. The mechanisms at the right column is obtained by opening the legs of the mechanisms left, and adding the end-effector between them. The complete parallel mechanisms are depicted in the right column.

The mechanism at the right top is shown at an equilibrium point above the ground because stresses are obtained within the legs. It can not move freely as its R-DoFs are non-parallel and thus are not rotating in the same plane. Looking from the perspective of the axis that is pointing inwards to the paper, the rigid links are rotating away from each other along a rotational path. This causes a pulling force at both sides of the end-effector in the horizontal direction. Manually pushing it through these equilibrium points causes a bistable motion as stresses are building up and released at this point. The motion tries to enlarge the closed loop of the mechanism in this bistable point in the stiff axial direction of the rigid links and the sliders. In comparison, the mechanism at the lower right is located at its bottom position (due to the gravity) as it can slide freely downwards because its R-axes are parallel. The motion is smooth because all rigid links are traveling a circular path in the same plane. No parts are moving away from each other in a constraint direction.

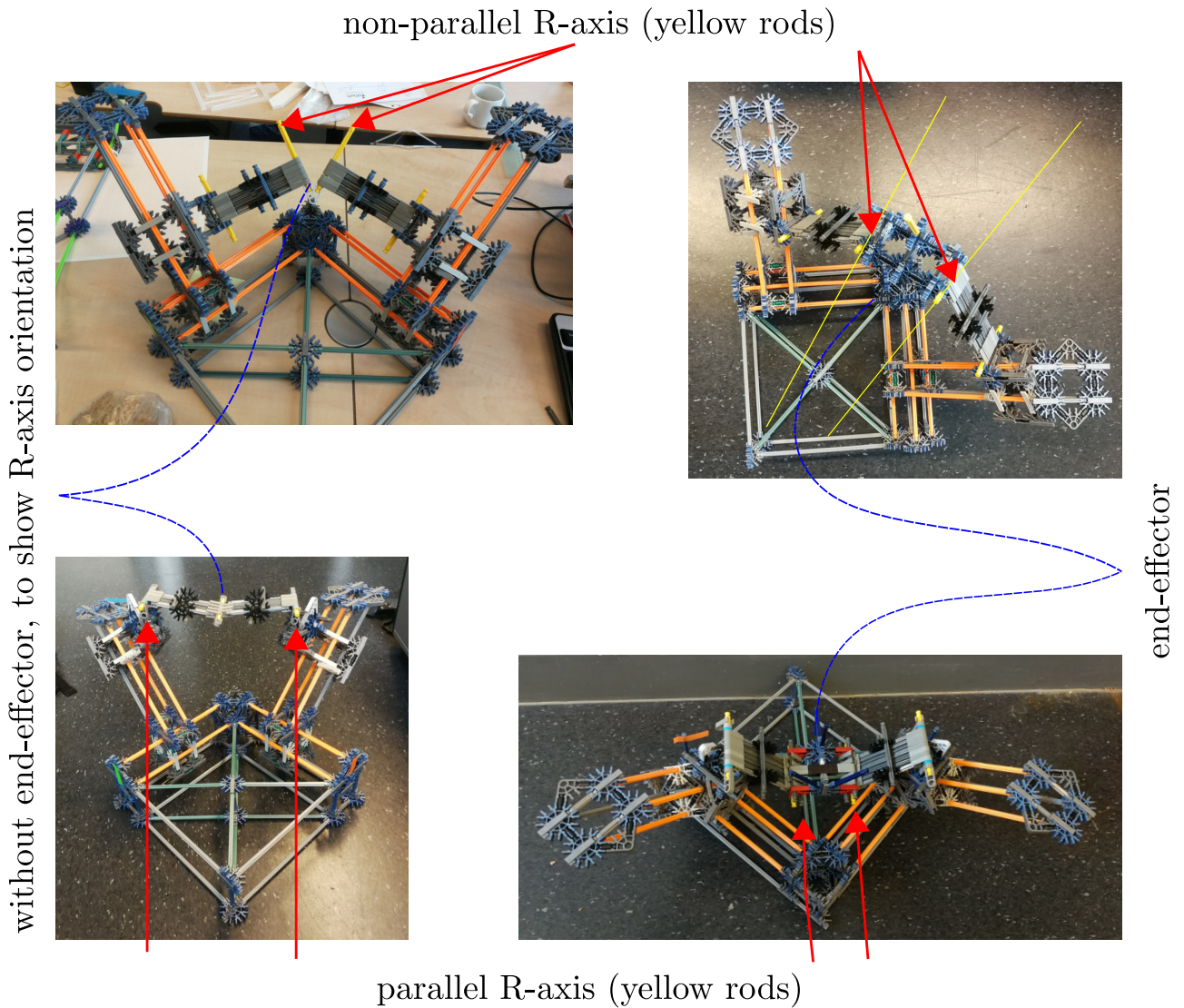


**Figure B-1:** Geometrical condition-1: The left column is added to show the orientation of the R-axis before the end-effector is connected between the legs. The resulting mechanisms after connection of the end-effector are shown in the right column. Right column; (top) mechanisms which can not move freely as its R-axes are non-parallel, (bottom) mechanisms which can move freely as its R-axes are parallel.

### B-1-1 Geometrical condition-1: compliant mechanism stiffening.

The same influence of geometrical condition-1 is observed within compliant mechanisms. The left picture of Figure B-2 shows a compliant mechanism (lego concept) with a leg on the right and the left side of the end-effector (lower part). In the left picture are the R-axes of the leg non-parallel w.r.t. each other as the upper axis are tilted under an angle w.r.t. the Z-axis while the lower R-axis of the leg are oriented in line with the z-axis. Moving the end-effector in the direction in- and outwards- of the page results in stiffening of the mechanism because the end-effector is also moving vertically due to the circular path around the two upper R-axes. The legs are pushing on the left and right side of the end-effector as a consequence of the z-component of the upper R-axis which can not be compensated by the lower R-axis. Therefore, the mechanisms can not move freely as internal stresses are induced as a result of the displacement component in the z-direction which tries to compress the end-effector. The mechanism on the right side of Figure B-2 has two parallel R-axes. The connected bodies (IMBD or end-effector) to each R-axis are moving among a circular path that is lying on two planes which are parallel. Both translational x-components during the rotation are compensating each other while no z-components are induced.

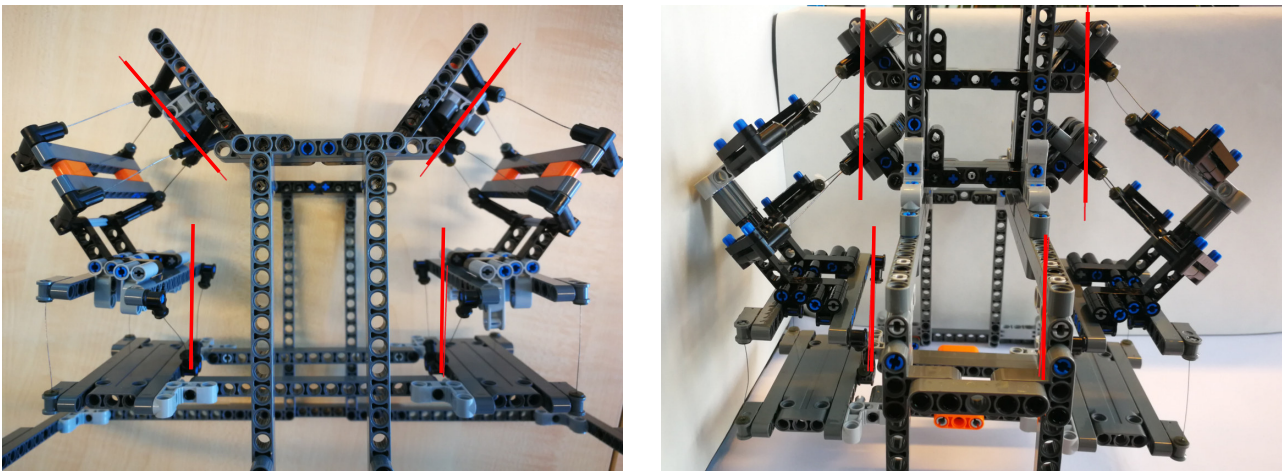


**Figure B-2:** Influence of geometrical condition G1 on the motion behavior of a compliant mechanism: Non-parallel R-axes, stiffening occur as the rotational motion of the IMBDs tries to compress the end-effector. The displacement components are both circular paths around the R-axes are not compensating each other. Mechanisms (right) has smooth motion because both circular paths are in the same plane, thus compensating each other displacement components as a result of the parallel R-axes.

## B-2 Geometrical condition-2

The influence of geometrical condition-2 is determined with the left mechanism as in Figure B-3, which is schematic draw in Figure B-4 (same as in previous appendix). The first slider ( $P_1$  at the ground) and the two revolute joints of the legs providing motion in the  $xy$ -plane (translation and rotation around  $z$ -axis). Only the second slider,  $P_2$ , (oriented vertically away from the ground in  $z$ -axis direction) is providing the motion in the  $Z$ -direction, thus this translational motion in the  $z$ -direction of the end-effector is a direct result of this slider and thus of the second geometrical condition-2, such as drawn in Figure B-3. Another variations is tested with the seconds slider of the leg in-line with the  $xy$ -plane resulting that motion in the  $z$ -direction occurs, which is schematic drawn in Figure B-5 and the right mechanism in Figure B-3.

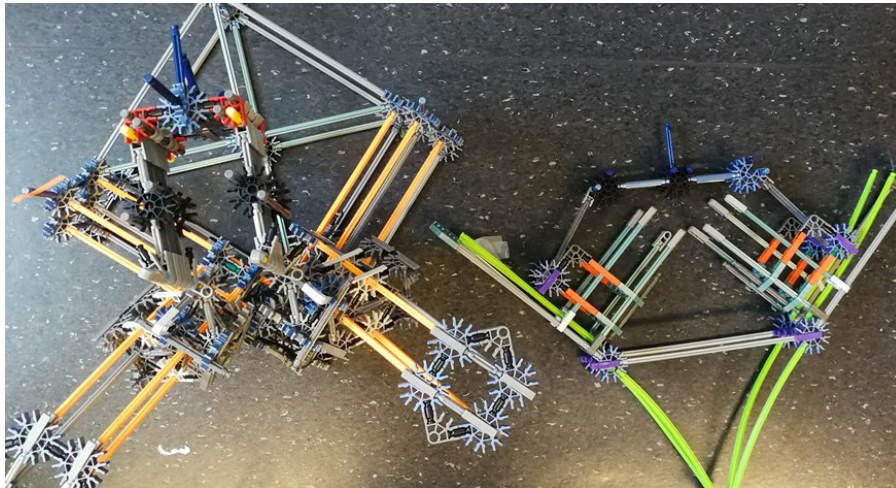


**Figure B-3:** Geometrical condition-2: Leftside, spatial TTTR-PM with one slider in  $z$ -direction (schematic drawing in Figure A-1) which satisfy geometrical condition-2. Rightside, Planar TTTR-PM with both sliders in one plane (schematic drawing in Figure B-5) which does not satisfy geometrical condition-2 thus no spatial translational motion.

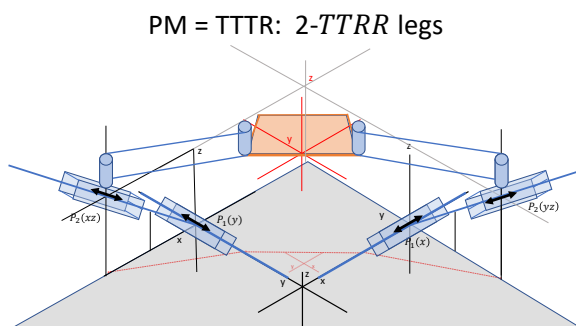


**Figure B-4:** Schematic drawing of K'nex toys model with two legs connected which satisfy geometrical condition-2. The leg comprises the following four joints, starting at the ground: first slider  $P_1$  (sequence starting at the ground) in  $xy$  plane, second slider  $P_2$  has a component in  $z$ -direction, followed by a two revolute joints connecting to the end-effector. In between a rigid link.

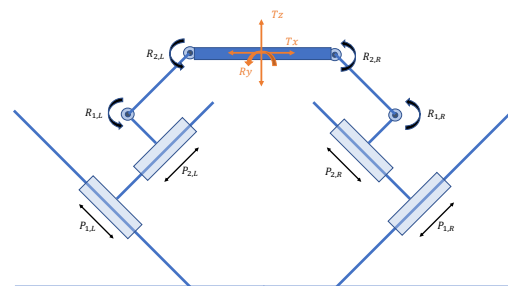


**Figure B-5:** Schematic drawing of planar K'nex toys model. The first and second sliders  $P_1$   $P_2$  (sequence starting at the ground) are in  $xy$ -plane, followed by a two revolute joints  $R_1$  and  $R_2$  connecting to the end-effector. In between a rigid link.

## Curk models of conceptual CLS I-V

The five Compliant Leg Solutions (CLS) which are synthesized using the COMAD-method for the manipulator with a TTTR-motion pattern are listed in Figure C-2. In the upper and middle row are the two constraint topologies listed. The CLS is listed in the lowest row and is obtained connecting the two topologies in series. The relative orientation of each constraint space with the world is determined in Section 4 of the article. From each compliant topology are four non-redundant wire constraints selected to construct the leg for which the selection criteria are found in Appendix E. In this Appendix, the motion behaviors are analyzed of the five legs. For this purpose, simple models are build using cork and spring-steel wires (diameter 0.5mm). The wires are inserted into the cork and due to its material properties (e.g. poisson ratio), they stay in place without being glued. The wire cork-models of each leg are stuck onto a green foam wall. The result is shown in Figure C-1 C-3 and C-4. Of course, this is only one leg and not a complete parallel compliant mechanism, but for selecting the best CLS concept this will be enough (otherwise, it will fall apart more easily because the parallel orientation of the R-axes must be assembled to precise to do properly by hand).

The legs are moved by hand in their four primary motion directions, translation in x,y, z-direction and rotation of the end-effector. The kinematic characteristics result in three classes of the legs based on their deformation behavior:

**manipulator cat. I:** *One topology of the leg is deforming* in the DoF similar to the displacement direction of the end-effector.

**manipulator cat. II/III:** *Both topologies of the leg are bending* in their R-DoF during displacement in the Ty-direction of the end-effector.

**manipulator cat. IV/V:** *One topology deforms due to torsion and one due to bending* both in their R-DoF during displacement in the Ty-direction of the end-effector.



**Figure C-1:** Five CLS concepts as curk prototypes: Initial position (Angled front view)

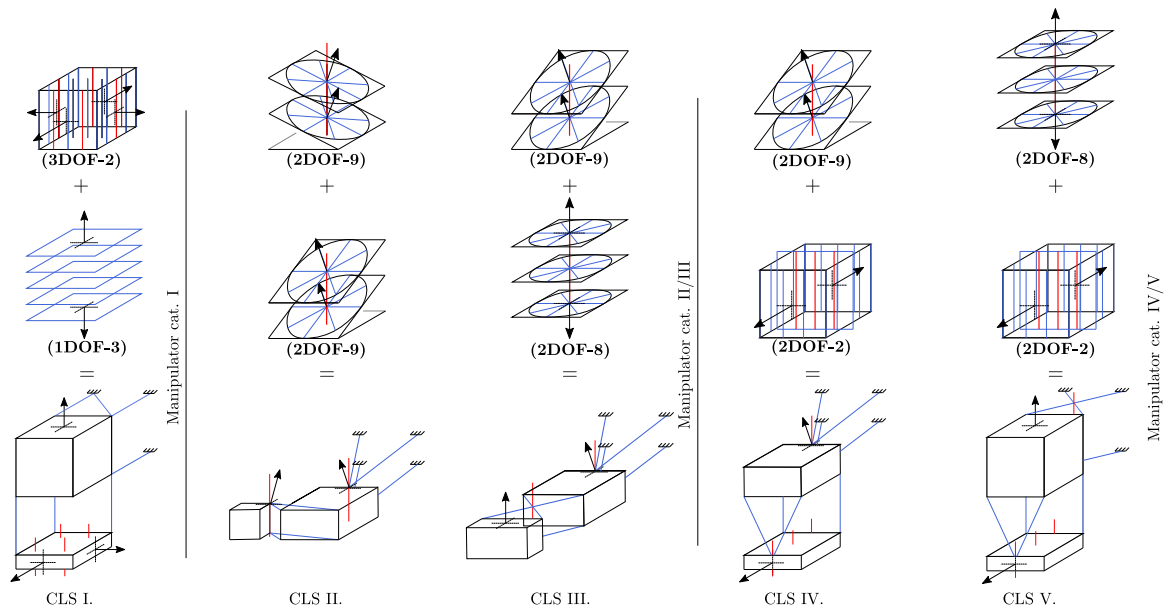


**Figure C-2:** The five Compliant Leg Solutions (CLS) which are synthesized using the COMAD-method for the manipulator with a TTTR-motion pattern in section 3 and 4 of the article. In the upper and middle row are the two constraint topologies listed which form the CLS when connected in seires. The complete CLS is listed in the lowest row. Connecting two CLSc in parallel result in the parallel compliant manipulator.

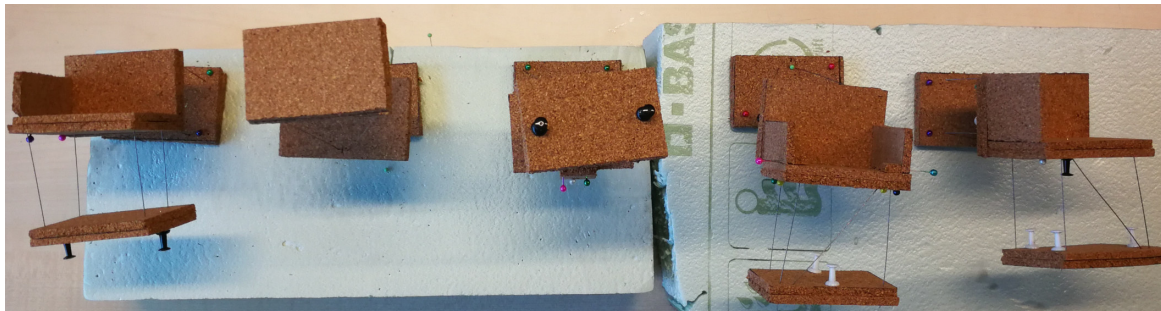


**Figure C-3:** Five CLS concepts as curk prototypes: Initial position (frontview)

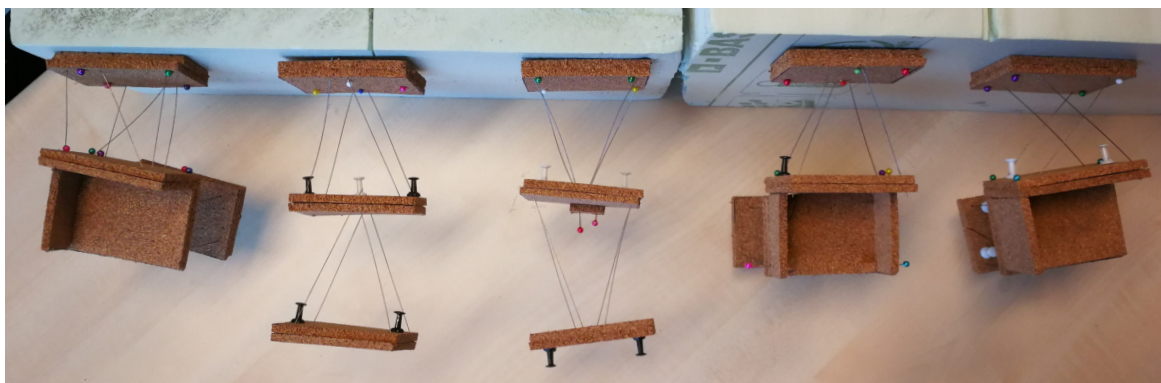


**Figure C-4:** Five CLS concepts as curk prototypes: Initial position (topview)

## C-1 Rotational deformation types

During the displacement in  $y$ -direction and rotation the motion is provided by deformation of the R-DoF of the topologies. Two different deformation types, bending and torsion, can be distinguished which results in a different motion of the connected body, therefore a small explanation about how rotation is obtained and why these topologies differ will be provided.

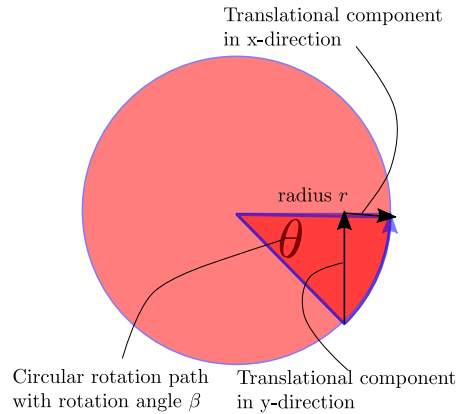


**Figure C-5:** Traveling along a circular path with angle  $\beta$  and radius  $r$  causing a change in the orientation with  $\beta$ . As consequence of the radius, also a change in the position in the  $x$ - and  $y$ -direction occur.

Figure C-5 shows a point at a circle with a rotational axis in the middle of the circle. The point travels along a circular path with angle  $\beta$  and radius  $r$  causing a change in the orientation with  $\beta$ . As a consequence of the radius, also a change in the position in the  $x$ - and  $y$ -direction occur. The rotational axis of a compliant element goes through the intersection point of all constraint lines. The rotational twist is obtained by deformation of the compliant element by bending or torsion, shown in Figure C-6. The wire constraints are stiff in their axial direction and compliant in all perpendicular directions.

Element **2DOF-2** is deforming by torsion because the (plane of) rotational axis lies parallel to planes of constraint lines. The body pivots on its own axis because the rotational torsion axis of the element goes through the connected body. The radius  $r = 0$  Element **2DOF-2** is compliant in the radial direction (the T-twist-direction) and stiff in the direction of the rotation axis.

The rotational axis of element **2DOF-8** and **2DOF-9** lies outside the connected body at distance  $r$ . The connected body orbits in a circular path  $\beta$  around the rotational axis and bends the connected wires of the element. Elements **2DOF-8** and **2DOF-9** are stiff in the radial direction and compliant in the direction of the rotational axis (the T-twist-direction).

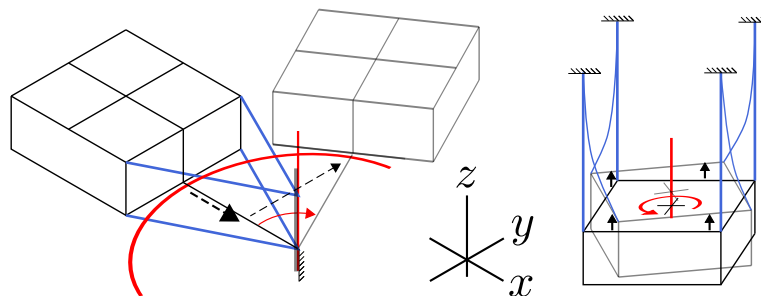


**Figure C-6:** The rotational twist occur by bending of the compliant element (left) or by torsion of the compliant element (right). Bending: the body orbits in a circular path in the  $XY$ -plane and has a translational  $T_y$ - and  $T_x$ -component (towards the R-axis). The direction of the R-axis is compliant and the radial direction stiff. Torsion: the body pivots on its own axis, is compliant in radial direction and stiff in axial direction.

## C-2 manipulator cat. I

The first category comprises CLS-1 as it is obtained by a serial kinematic solution legtype **3T1R**. Each primary motion direction is directly obtained by the deformation of one topology in a similar DoF, as is shown in FigureC-7. The left picture shows the deformation of the lower topology in a direction as a consequence of the displacement of the end-effector to the wall. The upper topology remains undeformed as the displacement is in its stiff axial direction. The middle picture shows the deformation upwards of the topology connected to the wall as a result of a displacement of the end-effector and IMBD upward. The right picture shows the deformation of the lower topology as a result of displacement to the right. For the rotational motion holds the same, the lower topology will deform. All in all is each displacement is obtained by one deformation in the similar DoF of the leg, just as was expected based on the freedom system which corresponds to the constraint topology. This distinguishes this CLS from the other four CLSs because their motion relies on two deformation topologies in series in DoFs which are unequal to the DoF of the displacement.

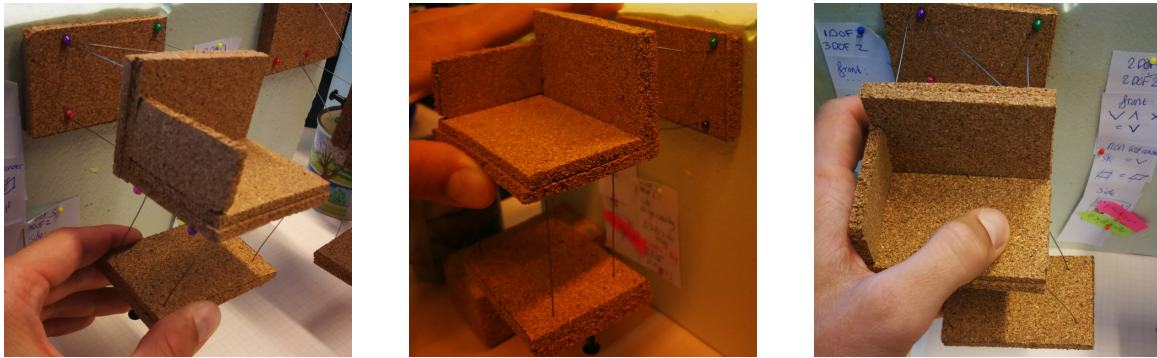


**Figure C-7:** The motion of CLS-I: Each displacement is obtained by the deformation of one topology in the direction of the same DoF. The result is that other topology (half of the leg) remains undeformed because the displacement of the is in its stiff direction. (left) translational displacement of the end-effector to the wall result in deformation of the lowest topology. (middle) upwards displacement of the end-effector and IMBD (stiff connected) by deformation of the top topology. (right) displacement to the right side of the end-effector results in the deformation of the lower topology.

### C-3 manipulator cat. II

Manipulator cat. II contains CLS-II and CLS-III because their R-DoFs are obtained by bending. Figure C-8 shows at the left the rotation motion of the end-effector connected at CLS-III. The IMBD and end-effector rotating in the same direction resulting in a summed contribution to rotational motion. In the right picture are the IMBD and end-effector counter-rotating as a consequence of a translational displacement to the side. Both changes in the orientation of the bodies will change each other resulting in a straight translation of the end-effector. However, the translational component in the x-direction as a consequence of the circular path is observed as a small displacement of the end-effector towards the green wall because it occurs in the stiff direction of both topologies.

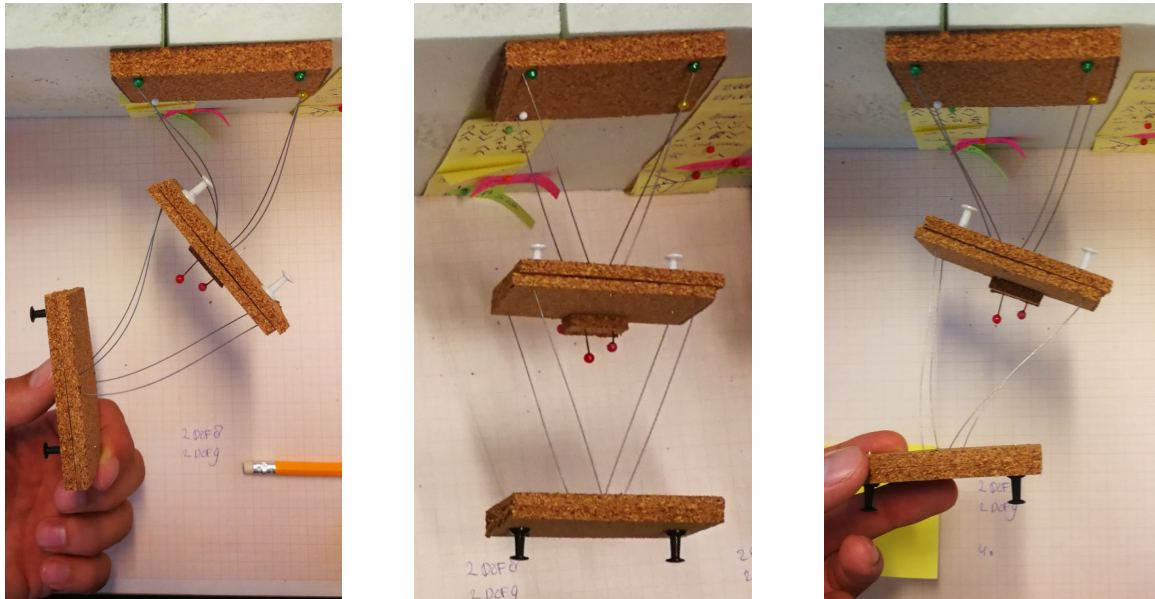


**Figure C-8:** The motion of CLS-III: Rotational displacement (left), undeformed initial position (middle), horizontal displacement motion in y-direction (right). Displacing the end-effector result in two deformations in series by bending of the topologies. In the left picture are the IMBD and end-effector rotating in the same direction resulting in a summed contribution to rotational motion. In the right picture are the IMBD and end-effector counter rotating and therefore canceling change in orientation of one and another resulting in a straight translation to the left side.

## C-4 manipulator cat. III

Manipulator cat. III contains CLS-IV and CLS-V because one of their R-DoF is obtained by bending and the other by torsion. Figure C-9 shows at the left the rotation motion of the end-effector connected at CLS-V. The IMBD and end-effector rotating in the same direction resulting in a summed contribution to rotational motion. The rotational motion is larger as in leg CLS-III because the wires are of topology **2DoF-8** are having a larger angle (crossing each other) and because the torsional motion is large as well. In the right picture are the IMBD and end-effector counter-rotating as a consequence of a translational displacement to the side. One translational component in the x-direction is observed in the foremost topology of the leg due to the circular path. However, this component is nicely canceled by the deformation of the posterior topology in its translational DoF (directed in the vertical).

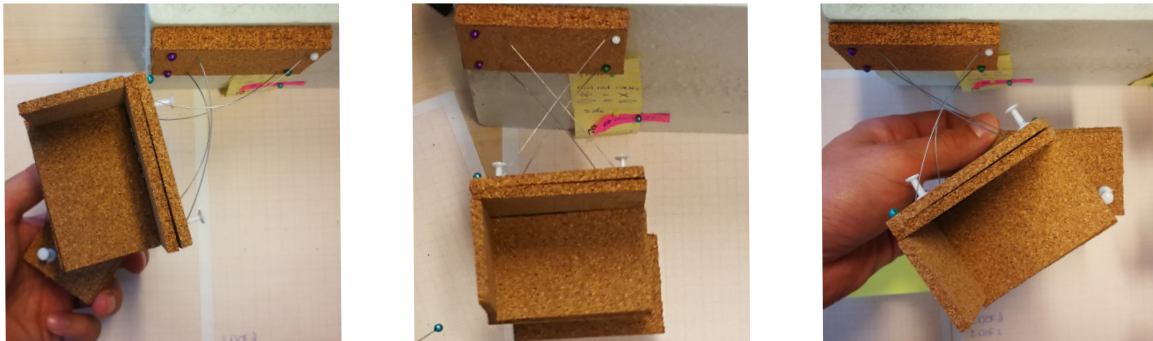


**Figure C-9:** The motion of CLS-V: Rotation displacement (left), undeformed initial position (middle), horizontal displacement in y-direction (right). Displacing the end-effector result a deformation by bending and one by torsion of the two serial topologies. In the left picture are the IMBD and end-effector rotating in the same direction resulting in a summed contribution to rotational motion. In the right picture are the IMBD and end-effector counter rotating and, therefore, canceling the change in orientation of one and another resulting in a straight translation to the left side.

All in all, three categories of CLS are made based on differences in deformation during motion. The difference in deformation will have an influence on the kinematics of the end-effector when connected in parallel, which will be discussed in more detail in section 4 of the article. The last two categories have two deforming topologies in series that enlarges the total displacement of the leg. The translational component in x-direction due to bending results in a translation of the end-effector for manipulator cat. II because it can not be canceled. However, in manipulator cat. III the translational component is canceled by the deformation of the **2DoF-2** topology in its T-DoF. This topology is simultaneously deformed by torsion.

# Conceptual variations in the configuration of the TTTR-manipulator

Different orientations and placements of the topologies are possible within the selected CLS-IV leg. The allowable variations are obtained within the set of free design variables. Despite that already the hanged and standing version were presented in the article, some additional concepts are build.

The sequence of topologies can be varied within the CLS-IV leg. In the left column of Figure D-1 is a configuration shown with topology **2DOF-2** connected to the end effector and in the right column of Figure D-1 a configuration with topology **2DOF-9** connected to the end effector. Comparing the mechanisms configuration of the left with the right column, it can be concluded that the left configuration has a much more compact design and a smaller end-effector. Therefore, this concept will be chosen.

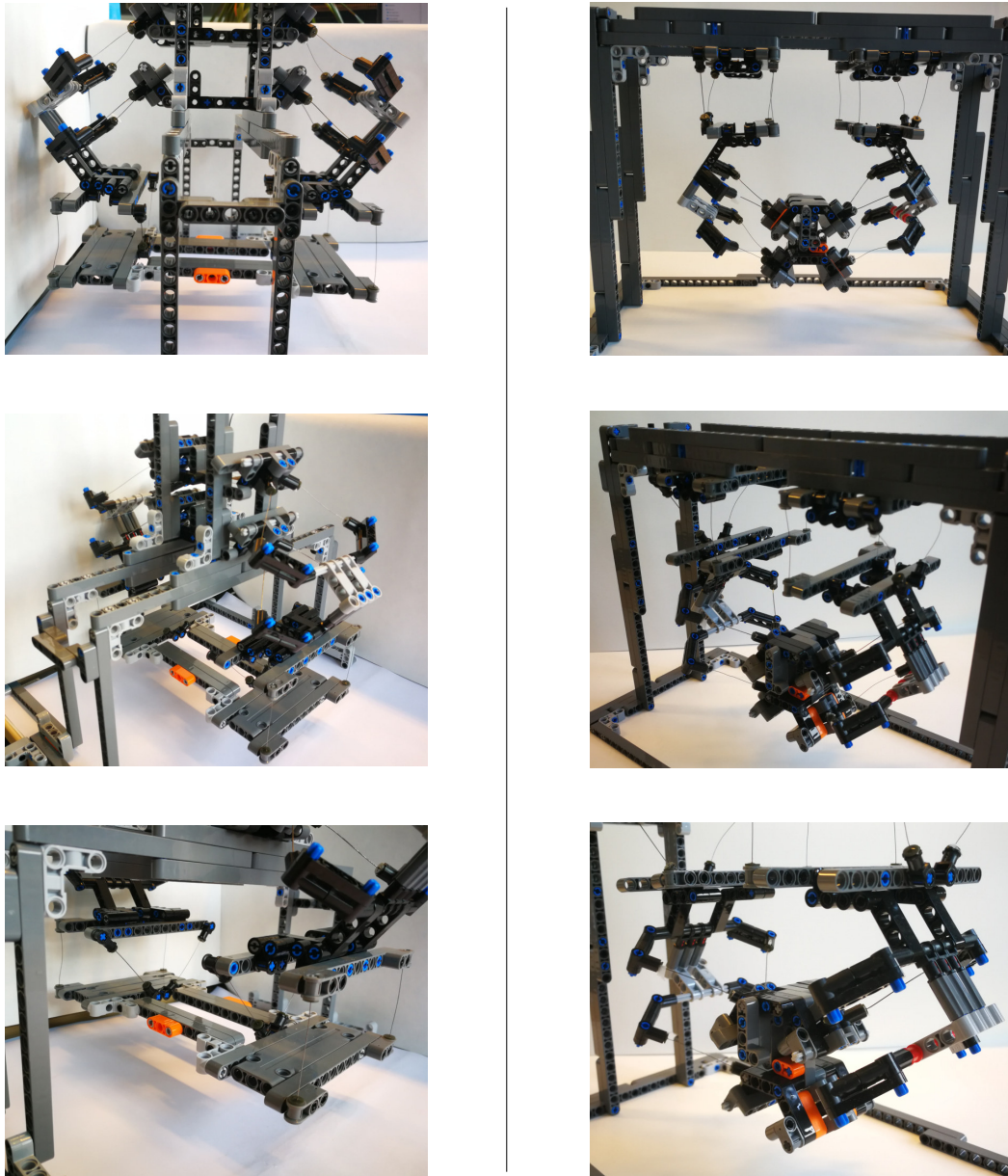


**Figure D-1:** Variation in the sequence of topologies in CLS-IV: In the left column is topology **2DOF-2** connected to the end effector and in the right column is topology **2DOF-9** connected to the end-effector. The end-effector of the left is larger than the end-effector on the right.

## Manufacturing of COMAD-demonstrator

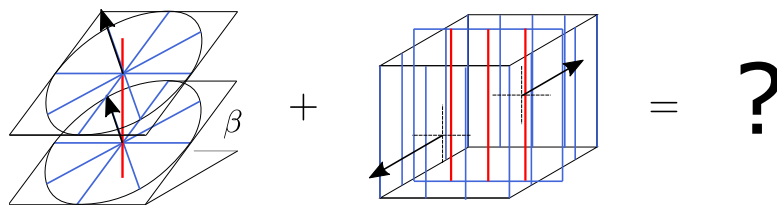
In this Appendix, the selected theoretical concept, of section 4 of the article, will be shaped and dimensioned to manufacture the demonstrator. First, the production method is prescribed. Secondly, the non-redundant wires will be selected from the constraint space. Thirdly, the fixation of the wires to the rigid bodies is designed. Finally, the material and dimensions of the wires and rigid bodies are specified to result in a producible demonstrator.

### E-1 Production method

As a production method is decided to assemble spring steel wires between 3D printed bodies instead of one monolithic printed design. The flexible elements are orientated at different angles and therefore will their properties fluctuate among each other due to the differently added layers of material. Spring steel wires are cheaper and more reliable because they have rarely the same material properties. However, a decent precision is necessary during the assembly of multiple parallel constraints between two bodies to avoid overconstrains or internal stresses.

### E-2 Selection of wires from the constraint topologies

The theoretical concept is selected in the article, however, only the serial chain of constraint space topologies are determined of the CLS, thus the result as in Figure E-1



CLS IV. (2DOF-9)(2DOF-2)

**Figure E-1:** The series of topologies is obtained, however the constraints are not selected from the compliant topology, thus the leg geometry is still undetermined

The wires are selected such that they tend to symmetry and be equally spread among the constraint space and thus among the connected body. Five options are provided in the FACT-method paper

for the selection of the wires from the planes of topology 2DOF-2 and 2DOF-9, which are listed in Figure E-2 and E-3. For topology 2DOF-9 four non-redundant wires are selected from the upper left picture, in order equally connect 2 wires at the top of the end effector and 2 wires at its bottom. The intersection point of the wires will be located at the edge of the end-effector to reduce its size and avoid collision of the wires, instead of an intersection half between the end-effector and the IMBD. For topology 2DOF-2 four non-redundant wires are selected from the middle lower picture, in order equally connect 2 wires at the front of the IMBD and 2 wires at its back. The wires of at the back are selected from the disk in order to increase the radial distance with the R-axis of topology 2DOF9 for a larger displacement while rotating.

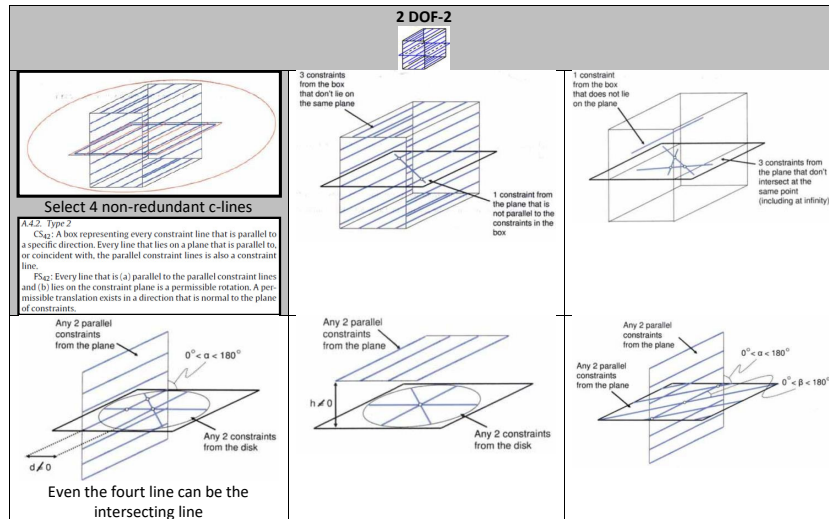


Figure E-2: Five possibilities to select four non-redundant wires from constraint topology 2DOF-2

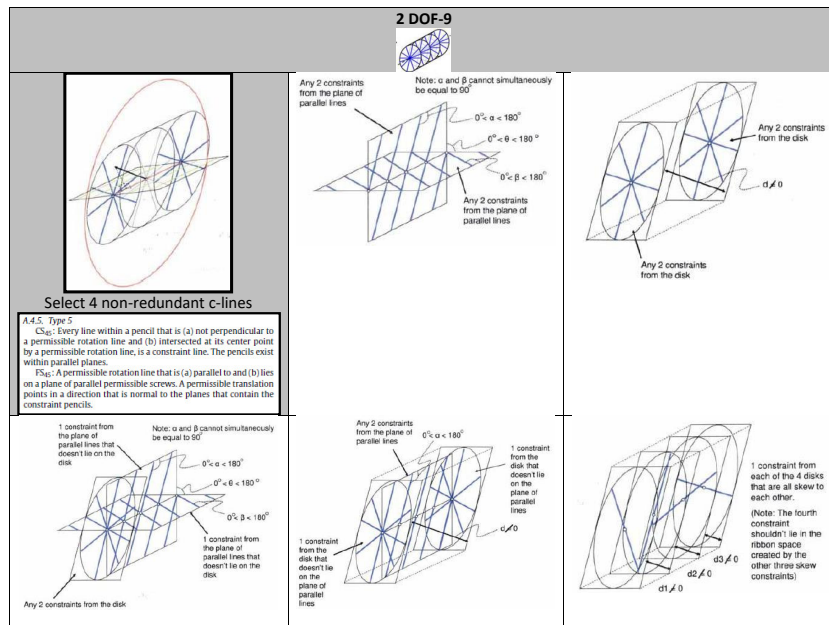
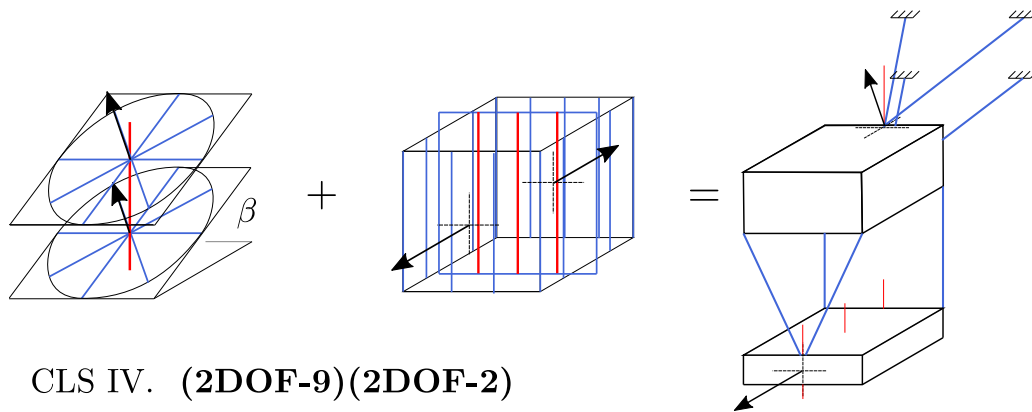


Figure E-3: Five possibilities to select four non-redundant wires from constraint topology 2DOF-9

Now the wires are selected the layout of the leg is determined such as shown in Figure E-4.



**Figure E-4:** The resulting CLS leg after selecting four wires per topology

### E-3 Design of the connection of the wires to the bodies

During the motions and deformations may the wire never slip along the connection point with the demonstrator thus the connection must be rigid and able to withstand significant forces. Clamping of the wires with a bolt towards rigid part of the bodies will fixate them properly. Clamping is advantageous compared to gluing as it can be disassembled and which stand higher forces (small gluing area due to the thin wires). A mechanism that can be disassembled is beneficial to avoid pre-stressing and deformation must be prevented while aligning 4x4 hand-cut wires in parallel between two rigid bodies with a specified orientation.

The wire will be clamped against a wall that will be printed as one piece with the body, such as shown in Figure E-5. The clamping is done by an M3 bolt-plate-nut connection which goes through the wall next to the wire. Instead of pushing the wire-end against the flat surface of the body, they are guided into a small tunnel within the body. This has two advantages, the orientation alignment of the wires between the bodies is better and pretension in the wire is prevented. The wires do not have to be pushed all the way to the bottom of the tunnel by which small inequalities in the lengths of hand-cut wires are forestalled and pre-stressing prevented.

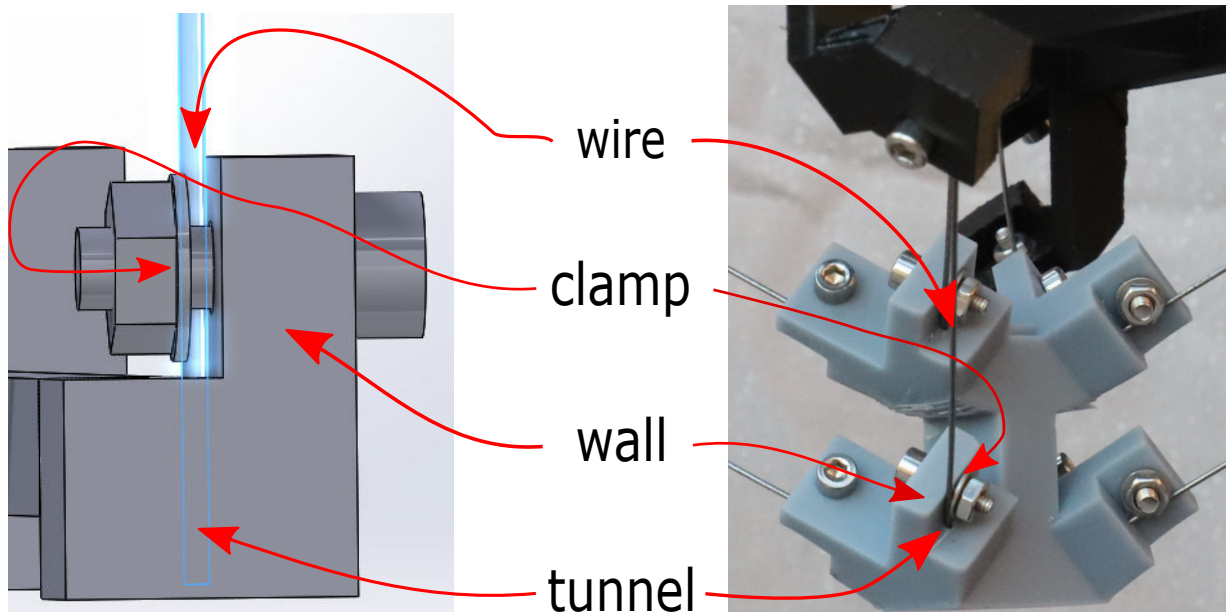


**Figure E-5:** Clamping of the wire using a bolt for connection. Guide the wire into the tunnels of both bodies for an aligned connection.

## E-4 Dimensioning

The spring steel wires have a thickness of 0.8mm. No calculations have been done, this thickness is selected, out of a set of 0.5, 0.6, 0.8, 1.0 and 1.5 mm wires diameters, and based on a tangible trade off between axial constraint stiffness and flexibility over a wire length of 100mm. For comparison, the lego and curk prototypes of the previous appendices are too compliant in all directions with a wire thickness of 0.3 and 0.5mm.

The four shorter wires, the only vertically orientated (positioned at the front of the IMBD), have a free-length of  $l_s = 87.5\text{mm}$  (+ 2x8mm of clamping + 2x7.5mm tunnel depth). The twelve remaining wires, do have an free-length of  $l_l = 100\text{mm}$  (+ 2x8mm of clamping + 2x7.5mm) tunnel depth and an angle of  $45^\circ$  with vertical-axis the IMBD or end-effector, such as shown in Figure E-6. The end-effector, the IMBD and the bodies at the ceiling, such dimensioned that they are connecting the end point of the four parallel wires of its corresponding constraint topology. The total volume of the prototype is,  $L \times W \times H = 145 \times 170 \times 170\text{mm}$ .

Pictures at different angles of the demonstrator are included below. The gray part is the end-effector, the two IMBDs are the two black bodies located in the middle of each leg, and two black rigid bodies at the top are for the connection with the rigid frame.

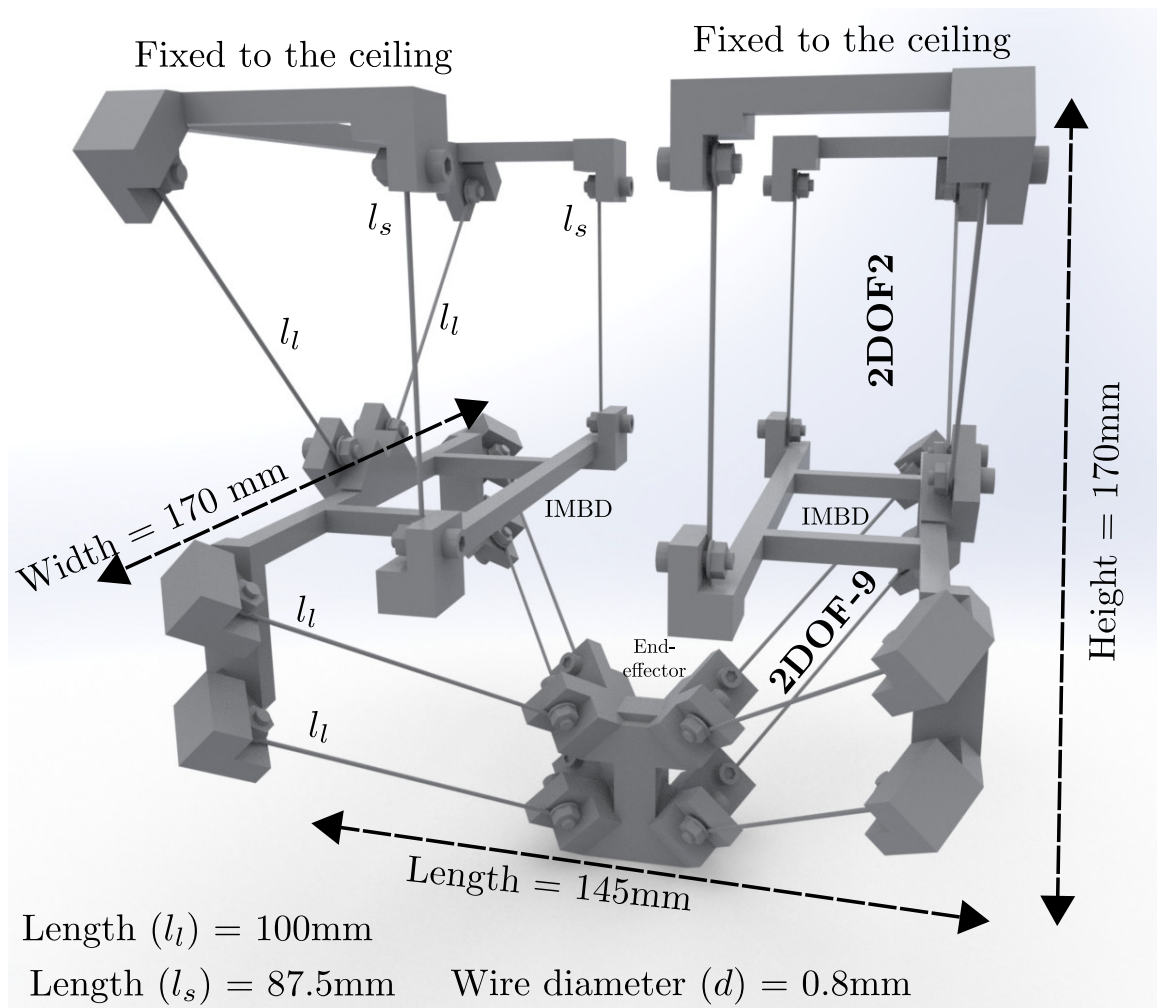


**Figure E-6:** Compliant manipulator concept, with 2 mirrored CLS-IV legs. End-effector below, two Intermediate Bodies (IMBD) in middle, attachment to ceiling. (Short) lengths of four vertical wires  $l_s = 87.5\text{mm}$ , (Long) lengths of twelfth angled wires  $l_l = 100\text{mm}$ . The length, Width, Height of the mechanism ( $L \times W \times H$ ) =  $145 \times 170 \times 170\text{mm}$

## E-5 Resulting demonstrator

Pictures at different angles of the demonstrator are included below. The gray part is the end-effector, the two IMBDs are the two black bodies located in the middle of each leg, and two black rigid bodies at the top are for the connection with the rigid frame, such as indicated in Figure E-7.

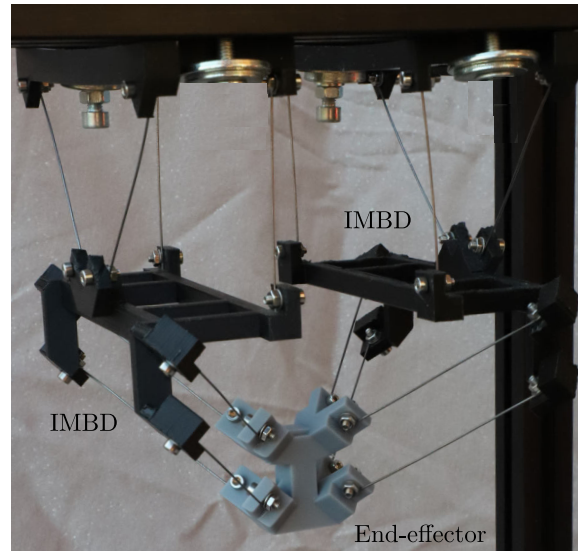


**Figure E-7:** The demonstrator: the selected hanging manipulator concept is with two mirrored CLS-V . Topology- $(2\text{DOF} - 2)_1$  is connected to the ceiling and topology- $(2\text{DOF} - 9)_2$  to the end-effector (gray). The topologies of the CLS are connected by the black intermediate rigid body (IMBD).

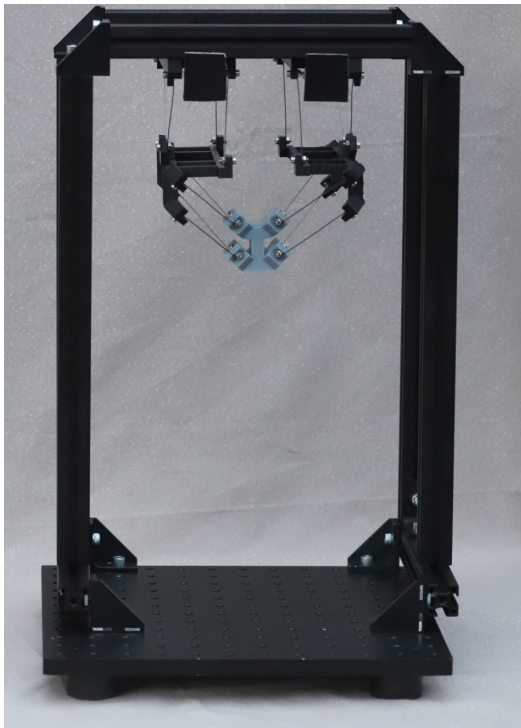


**Figure E-8:** Demonstrator frame set up (Frontview); Gray body is end-effector, two black bodies the IMBDs.



**Figure E-9:** Demonstrator frame set up (Frontview at an angle); Gray body is end-effector, two black bodies the IMBDs.

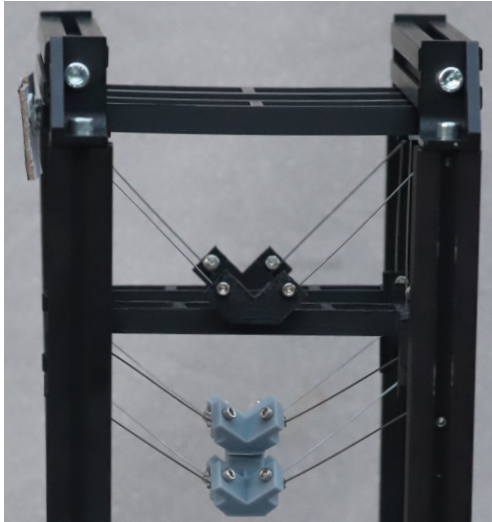


**Figure E-10:** Demonstrator (Sideview); Gray body is end-effector, two black bodies the IMBDs.



**Figure E-11:** Demonstrator (Topview); Gray body is end-effector, two black bodies the IMBDs.

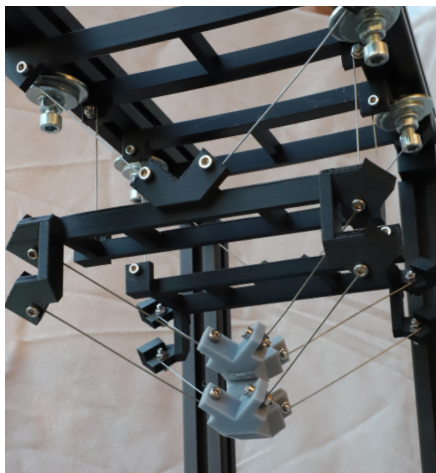


**Figure E-12:** Demonstrator (side and bottom angle view); Gray body is end-effector, two middle black bodies the IMBDs.

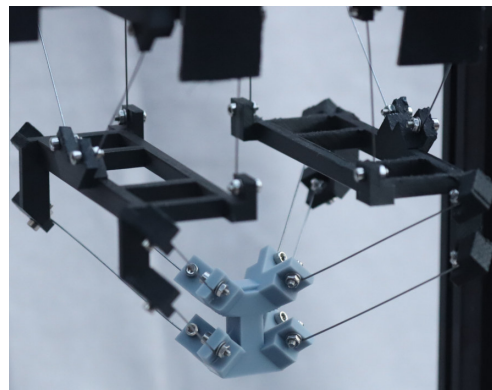


**Figure E-13:** Demonstrator (front and top angle view); Gray body is end-effector, two black bodies the IMBDs.

## E-6 Experimental evaluation and test set up

This section provide the test set up used during the the four tests of the experimental evaluation of the demonstrator. A fishing wire is attached to the end-effector. The displacement is imposed by manually pulling the end-effector from its initial position towards one of the four primary directions respectively, until the deformation or pulling force feels disproportionate. The result is photographed from which the total displacement is determined using a grid paper (block size 5mm) behind the demonstrator. Photos of the test set up are provided in Figure E-14.

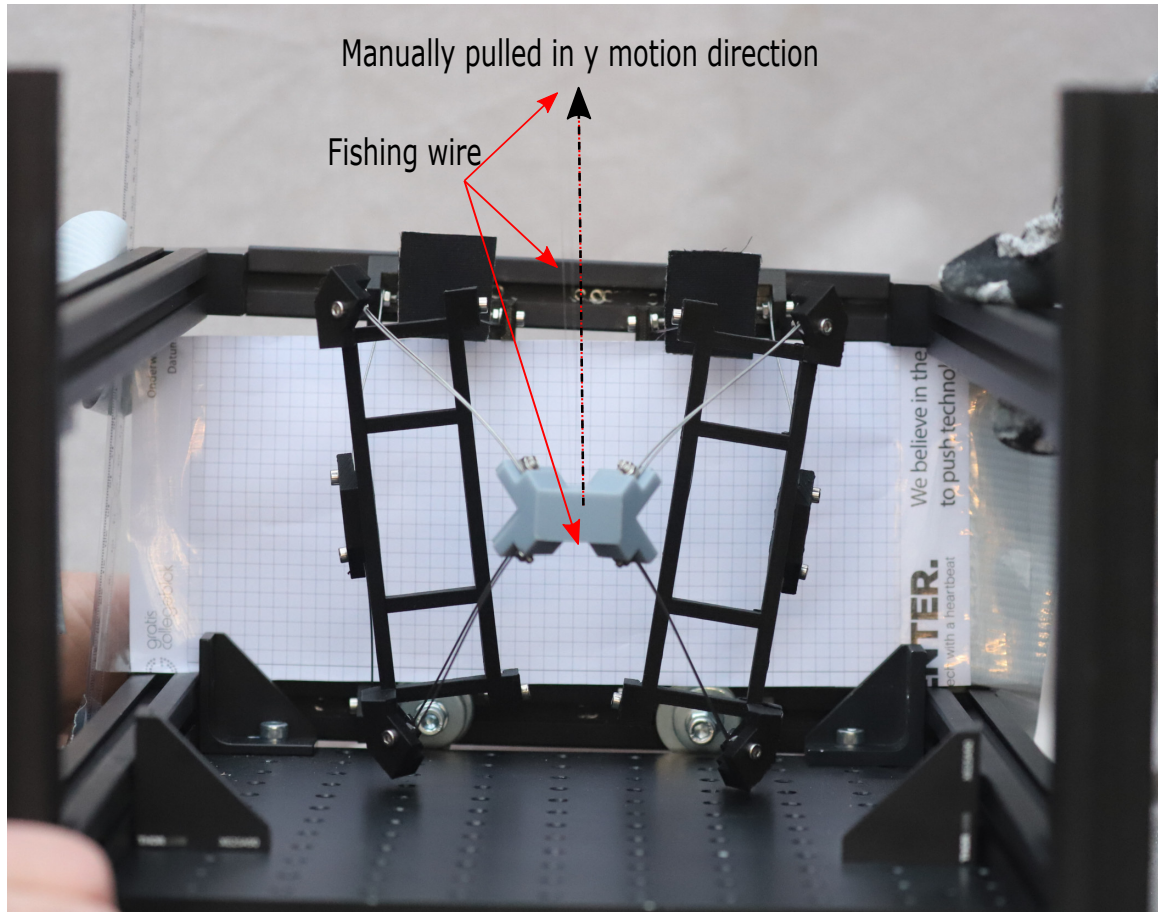


**Figure E-14:** Test set up from below the end-effector. A fishing wire (hardly visible, but located between three red solid arrow lines) is around the end-effector (gray body) and is manually pulled in the y-direction for the primary  $T_y$  translational motion

---

# Bibliography

- [1] B. Siciliano and O. Khatib, *Springer handbook of robotics*. Springer, 2016.
- [2] N. Applied and E. Sciences, “Cognitive robots for flexible agro food technology (flexcraft),” *Unpublished*, 2017.
- [3] L. L. Howell, *Compliant mechanisms*. John Wiley & Sons, 2001.
- [4] L. L. Howell, S. P. Magleby, B. M. Olsen, and J. Wiley, *Handbook of compliant mechanisms*. Wiley Online Library, 2013.
- [5] S. Henein, P. Spanoudakis, S. Droz, L. I. Myklebust, and E. Onillon, “Flexure pivot for aerospace mechanisms,” in *10th European Space Mechanisms and Tribology Symposium, San Sebastian, Spain*, pp. 285–288, 2003.
- [6] S. T. Smith, *Flexures: elements of elastic mechanisms*. Crc Press, 2014.
- [7] M. Berglund, S. Magleby, and L. Howell, “Design rules for selecting and designing compliant mechanisms for rigid-body replacement synthesis,” in *Proceedings of the 26th Design Automation Conference, ASME DETC, Baltimore, MD*, vol. 14225, 2000.
- [8] M. Pucheta and A. Cardona, “Kinematics synthesis of compliant mechanisms using rigid-body replacement,” *Multibody Dynamics*, pp. 156–157, 2007.
- [9] X. Kong and C. M. Gosselin, *Type synthesis of parallel mechanisms*, vol. 33. Springer, 2007.
- [10] J. B. Hopkins and M. L. Culpepper, “Synthesis of multi-degree of freedom, parallel flexure system concepts via freedom and constraint topology (fact)–part i: Principles,” *Precision Engineering*, vol. 34, no. 2, pp. 259–270, 2010.
- [11] J. B. Hopkins and M. L. Culpepper, “Synthesis of precision serial flexure systems using freedom and constraint topologies (fact),” *Precision Engineering*, vol. 35, no. 4, pp. 638–649, 2011.

